

# Assimilation of Carbonyl Sulfide (COS) fluxes within the adjoint-based data assimilation system—Nanjing University Carbon Assimilation System (NUCAS v1.0)

Huajie Zhu<sup>1</sup>, Mousong Wu<sup>1\*</sup>, Fei Jiang<sup>1,2,3,4</sup>, Michael Vossbeck<sup>5</sup>, Thomas Kaminski<sup>5</sup>, Xiuli Xing<sup>6</sup>, Jun Wang<sup>1</sup>, Weimin Ju<sup>1</sup>, Jing M. Chen<sup>7</sup>

<sup>1</sup>International Institute for Earth System Science, Nanjing University, Nanjing, 210023, China

<sup>2</sup>Jiangsu Provincial Key Laboratory of Geographic Information Science and Technology, School of Geography and Ocean Science, Nanjing University, Nanjing, 210023, China

<sup>3</sup>Key Laboratory for Land Satellite Remote Sensing Applications of Ministry of Natural Resources, School of Geography and Ocean Science, Nanjing University, Nanjing, 210023, China

<sup>4</sup>Frontiers Science Center for Critical Earth Material Cycling, Nanjing University, Nanjing, 210023, China

<sup>5</sup>The Inversion Lab, Hamburg, Germany

<sup>6</sup>Fudan University, Shanghai, 200437, China

<sup>7</sup>Department of Geography and Program in Planning, University of Toronto, ON M5S 3G3, Canada

15

Correspondence: Mousong Wu (mousongwu@nju.edu.cn)

**Abstract.** Modeling and predicting changes in the function and structure of the terrestrial biosphere and its feedbacks to climate change strongly depends on our ability to accurately represent interactions of the carbon and water cycles, and energy exchange. However, carbon fluxes, hydrological status and energy exchange simulated by process-based terrestrial ecosystem models are subject to significant uncertainties, largely due to the poorly calibrated parameters. In this work, an adjoint-based data assimilation system (Nanjing University Carbon Assimilation System, NUCAS v1.0) was developed, which is capable of assimilating multiple observations to optimize process parameters of a satellite data driven ecosystem model—BEPS (Biosphere-atmosphere Exchange Process Simulator). Data assimilation experiments were conducted to investigate the robustness of NUCAS, and to test the feasibility and applicability of assimilating carbonyl sulfide (COS) fluxes from seven sites, to enhance our understanding of stomatal conductance and photosynthesis. Results showed that NUCAS is able to achieve a consistent fit to COS observations across various ecosystems, including evergreen needleleaf forest, deciduous broadleaf forest, C3 grass and C3 crop. Comparing model simulations with validation datasets, we found that assimilating COS fluxes notably improves the model performance in gross primary productivity and evapotranspiration, with average root mean square error (RMSE) reductions of 23.54% and 16.96%, respectively. We also showed that NUCAS is capable of constraining parameters through assimilating two sites simultaneously and achieving a good consistency with single-site assimilation. Our results demonstrate that COS can provide constraints on parameters relevant to water, energy and carbon processes with the data assimilation system, and opens new perspectives for better understanding of the ecosystem carbon, water and energy exchanges.

25

30

**Keywords:** Carbonyl sulfide; Data assimilation; Carbon cycle; Satellite-driven; Ecosystem model

## 35 1 Introduction

Overwhelmingly due to anthropogenic fossil fuel and carbonate emissions, as well as land use and land cover change (Arias et al., 2021), atmospheric carbon dioxide (CO<sub>2</sub>) concentrations have increased at an unprecedented rate since the Industrial Revolution and the global climate has been profoundly affected. As a key component of earth system, the terrestrial biosphere has absorbed about 30% of anthropogenic CO<sub>2</sub> emissions since 1850 (Friedlingstein et al., 2022). However, in line with large-scale global warming, the structure and function of the terrestrial biosphere have changed rapidly (Grimm et al., 2013;

40

Arias et al., 2021; Moore and Schindler, 2022). As a consequence, terrestrial carbon fluxes are subject to great uncertainty (Macbean et al., 2022).

45 Terrestrial ecosystem models have been an important tool used to investigate the net effect of complex feedback loops between the global carbon cycle and climate change (Zaehle et al., 2005; Fisher et al., 2014; Fisher and Koven, 2020). Meanwhile, with the advancement of modern observational techniques, a rapidly increasing number of satellite- and ground-based observational datasets have played an important role in studying the spatiotemporal distribution and mechanisms of the terrestrial ecosystem carbon fluxes (Rodell et al., 2004; Quirita et al., 2016). Observations (Scholze et al., 2017), such as sun-induced chlorophyll fluorescence (Schimel et al., 2015) and soil moisture (Wu et al., 2018), have been used to estimate or constrain carbon fluxes in terrestrial ecosystems. Carbonyl sulfide (COS) has emerged as a promising proxy for understanding terrestrial carbon uptake and plant physiology (Montzka et al., 2007; Campbell et al., 2008) since it is taken up by plants through the same pathway of stomatal diffusion as CO<sub>2</sub> (Goldan et al., 1988; Sandoval-Soto et al., 2005; Seibt et al., 2010) and completely removed by hydrolysis without any back-flux in leaves under normal conditions (Protoschill-Krebs et al., 1996; Stimler et al., 2010).

50 Plants open/close leaf stomata in order to regulate the water and CO<sub>2</sub> transit during transpiration and photosynthesis (Daly et al., 2004). As an important probe for characterizing stomatal conductance, COS has shown great potential to constrain plant photosynthesis and transpiration and to improve understanding of the water-carbon coupling (Wohlfahrt et al., 2012; Asaf et al., 2013; Wehr et al., 2017; Kooijmans et al., 2019; Sun et al., 2022; Zhu et al., 2024). A number of empirical or mechanistic COS plant uptake models (Campbell et al., 2008; Wohlfahrt et al., 2012; Berry et al., 2013) and soil exchange models (Kesselmeier et al., 1999; Berry et al., 2013; Launois et al., 2015; Sun et al., 2015; Whelan et al., 2016; Ogée et al., 2016; Whelan et al., 2022) have been developed to simulate COS fluxes in order to more accurately estimate gross primary productivity (GPP), stomatal conductance as well as transpiration. However, due to the lack of ecosystem-scale measurements of the COS flux (Brühl et al., 2012; Wohlfahrt et al., 2012; Kooijmans et al., 2021), only few studies were conducted to systematically assess the ability of COS to simultaneously constrain photosynthesis, transpiration and other related processes in ecosystem models.

60 Data assimilation is an approach that aims at producing physically consistent estimates of the dynamical behaviour of a model by combining information in process-based models and observational data (Liu and Gupta, 2007; Law et al., 2015). It has been widely applied in geophysics and numerical weather prediction (Tarantola, 2005). In the past few decades, substantial efforts have been put into the use of satellite- (Knorr et al., 2010; Kaminski et al., 2012; Deng et al., 2014; Scholze et al., 2016; Norton et al., 2018; Wu et al., 2018) and ground-based (Knorr and Heimann, 1995; Rayner et al., 2005; Santaren et al., 2007; Kato et al., 2013; Zobitz et al., 2014) observational datasets to constrain or optimize the photosynthesis, transpiration and energy-related parameters and variables of terrestrial ecosystem models via data assimilation techniques. More specifically, by applying data assimilation methods to process-based models, not only can the observed dynamics of ecosystems be more accurately portrayed, but also our understanding of ecosystem processes can be deepened, with respect to their responses to climate changes (Luo et al., 2011; Keenan et al., 2012; Niu et al., 2014).

75 In this study, we present the newly developed adjoint-based Nanjing University Carbon Assimilation System (NUCAS v1.0). NUCAS v1.0 is designed to assimilate multiple observational data streams, including COS fluxes, to improve the process-based Biosphere-atmosphere Exchange Process Simulator (BEPS) (Liu et al., 1997), which has been specifically extended for simulating the ecosystem COS flux with the advanced two-leaf model that is driven by satellite observations of leaf area index (LAI).

In this context, the main questions that we aim to answer in this paper are:

80 What parameters is the COS simulation sensitive to and how do these parameters change in the assimilation of ecosystem-scale COS fluxes?

How effective is the assimilation of COS fluxes in improving the carbon, water and energy balance for different ecosystems (including Evergreen needleleaf forest, deciduous broadleaf forest, C3 grass and C3 crop)?

85 Which processes are constrained by the assimilation of COS fluxes and what are the mechanisms leading to adjustments of the corresponding process parameters?

How robust is the NUCAS when optimizing over single-site and over two sites simultaneously?

To achieve these objectives, COS flux observations across a wide range of ecosystems (including evergreen needleleaf forest, deciduous broadleaf forest, C3 grass and C3 crop) are assimilated into NUCAS to optimize the model parameters using the four-dimensional variational (4D-Var) data assimilation approach, and the optimization results are evaluated against *in situ* observations. Materials and methods used in our study are described in Section 2, such as the BEPS model and NUCAS, are introduced, along with the data used to drive BEPS and assimilated into NUCAS, and the parameters chosen to be optimized in this study. The results are presented in Section 3, including the fit of COS simulations to observations, the variation and impact of parameters on simulated COS, as well as the comparison and evaluation of model outputs. Section 4 discusses the impacts of the COS assimilation on parameters and processes related to the water-carbon cycle and energy exchange as well as the influence of uncertainty inputs, in particular impacts of LAI on posterior parameters values. In addition, caveats and implications of assimilating COS flux are summarized. Finally, conclusions are laid out in Section 5.

## 2 Materials and Methods

### 2.1 NUCAS data assimilation system

#### 2.1.1 NUCAS framework

100 NUCAS is built around the generic satellite data driven ecosystem model BEPS, and applies the 4D-Var data assimilation method (Talagrand and Courtier, 1987). The BEPS model uses satellite-derived one-sided LAI to drive the phenology dynamics and separates sunlit and shaded leaves in calculating canopy-level energy fluxes and photosynthesis. It further features detailed representations of water and energy processes (**Figure 1**). These features render BEPS more advanced in representing ecosystem processes than standard ecosystem models (Richardson et al., 2012) with less parameters to be calibrated owing to the LAI-driven phenology.

Data assimilation is performed in two sequential steps: first, an inversion step adjusts the values of parameters controlling photosynthesis, energy balance, hydrology and soil biogeochemical processes to match the observations. Second, the posterior parameters obtained in the first step are used as input data for the second step, in which the BEPS model is re-run to obtain the posterior model variables. The schematic of the system is shown in **Figure 1**.

110 Considering model and data uncertainties, NUCAS implements a probabilistic inversion concept (Talagrand and Courtier, 1987; Tarantola, 1987; Tarantola, 2005) by using Gaussian probability density functions to combine the dynamic model and observations to obtain an estimate of the true state of the system and model parameters (Talagrand, 1997; Dowd, 2007). Hereby, we minimize the following cost function:

$$J(x) = \frac{1}{2} \left[ (M(x) - O)^T C_o^{-1} (M(x) - O) + (x - x_0)^T C_x^{-1} (x - x_0) \right] \quad (1)$$

115 where O and M denote vectors of observations and their modelled counterparts, respectively;  $x$  and  $x_0$  denotes the control parameter vector with current and prior values, respectively.  $C_o$  and  $C_x$  denote the uncertainty covariance matrices for observations and prior parameters. Both matrices are diagonal expressing the assumption that observation uncertainties and the parameter uncertainties to be independent (Rayner et al., 2005). This definition of the cost function contains both the

mismatch between modelled and observed COS fluxes and the mismatch between current and prior parameter values (Rayner et al., 2005).

To determine an optimal set of parameters which minimizes  $J$ , a gradient-based optimization algorithm performs an iterative search (Wu et al., 2020). In each iteration, the gradient of  $J$  is calculated by applying the adjoint of the model, where the model is run backward to efficiently compute the sensitivity of  $J$  and with respect to  $x$  (Rayner et al., 2005). The gradient of  $J$  is used to define a new search direction. The adjoint model is an efficient sensitivity analysis tool for calculating the parametric sensitivities of complex numerical model systems (An et al., 2016). The computational cost of it is independent of the number of parameters and is in the current case comparable to 3–4 evaluations of  $J$ . In this study, all derivative code is generated from the model code by the automatic differentiation tool TAPENADE (Hascoët and Pascual, 2013). The derivative with respect to each parameter was validated against finite differences of model simulations, which showed agreement within the accuracy of the finite difference approximation. The minimization of the cost function is implemented in a normalized parameter space where the parameter values are measured in multiples of their respective standard deviation with Gaussian priors (Kaminski et al., 2012). The model parameters are the various constants that are not influenced by the model state. Therefore, while they may change between plant function types (PFTs) to reflect different conditions and physiological mechanisms, they will not change in time (Rayner et al., 2005).

### 2.1.2 BEPS basic model

The BEPS model (Liu et al., 1997; Chen et al., 1999; Chen et al., 2012) is a process-based diagnostic model driven by remotely sensed vegetation data, including LAI, clumping index, and land cover type, as well as meteorological and soil data (Chen et al., 2019). With the consideration of coupling among terrestrial carbon, water, and nitrogen cycles (He et al., 2021), the BEPS model now consists of photosynthesis, energy balance, hydrological, and soil biogeochemical modules (Ju et al., 2006; Liu et al., 2015). It stratifies whole canopies into sunlit and shaded leaves to calculate carbon uptake and transpiration for these two groups of leaves separately (Liu et al., 2015). For each group of leaves, the GPP is calculated by scaling Farquhar's leaf biochemical model (Farquhar et al., 1980) up to canopy-level with a updated temporal and spatial scaling scheme (Chen et al., 1999), and the stomatal conductance is calculated using a modified version of the Ball–Berry (BB) model (Ball et al., 1987; Ju et al., 2006). Evapotranspiration is calculated as the summation of sunlit leaf and shaded leaf transpirations, evaporation from soil and wet canopy, and sublimation from snow storage on the ground surface (Liu et al., 2003). The BEPS model stratifies the soil profile into multiple layers (five were used in this study), and simulates temperature and water content from each layer (Ju et al., 2006). The soil water content is then used to adjust stomatal conductance considering the water stress impacts (Ju et al., 2010; He et al., 2021). Over the last few decades, the BEPS model has been continuously improved and used for a wide variety of terrestrial ecosystems (Schwalm et al., 2010; Liu et al., 2015).

The previous version of BEPS considers a total of six PFTs as well as eleven soil textures (Chen et al., 2012). We use the same soil texture but added four PFTs to BEPS in order to better discriminate vegetation types, especially the C4 grass and C4 crop. Detailed information on these ten PFTs and eleven soil textures is given in **Table S1**.

### 2.1.3 COS modelling

The ecosystem COS flux,  $F_{COS,ecosystem}$ , includes both plant COS uptake  $F_{COS,plant}$  and soil COS flux exchange  $F_{COS,soil}$  (Whelan et al., 2016). In this study, these two components were modelled separately. The canopy-level COS plant uptake  $F_{COS,plant}$  ( $\text{pmol m}^{-2} \text{s}^{-1}$ ) was calculated by upscaling the resistance analog model of COS uptake, as presented by Berry et al. (2013) with the upscaling scheme recommended by Chen et al. (1999). Specifically, considering the different responses of foliage to diffuse and direct solar radiation (Gu et al., 2002),  $F_{COS,plant}$  is calculated as:

$$F_{cos,plant} = F_{cos,sunlit}LAI_{sunlit} + F_{cos,shaded}LAI_{shaded} \quad (2)$$

where  $LAI_{sunlit}$  and  $LAI_{shaded}$  are the LAI values ( $m^2 m^{-2}$ ) of sunlit and shaded leaves, respectively.  $F_{COS,sunlit}$  and  $F_{COS,shaded}$  are the leaf-level COS uptake rate ( $pmol m^{-2} s^{-1}$ ) of sunlit and shaded leaves, respectively. The leaf-level COS uptake rate  $F_{COS,leaf}$  is calculated as:

$$F_{COS,leaf} = COS_a * \left( \frac{1.94}{g_{sw}} + \frac{1.56}{g_{bw}} + \frac{1}{g_{COS}} \right)^{-1} \quad (3)$$

where  $COS_a$  is the COS mole fraction in the bulk air and  $g_{sw}$  and  $g_{bw}$  are the stomatal conductance and leaf laminar boundary layer conductance to water vapor ( $H_2O$ ), respectively (Berry et al., 2013). The factors 1.94 and 1.56 account for the smaller diffusivity of COS with respect to  $H_2O$  (Seibt et al., 2010; Stimler et al., 2010). The apparent conductance for COS uptake from the intercellular airspaces is denoted by  $g_{COS}$  and combines the mesophyll conductance and the biochemical reaction rate of COS and carbonic anhydrase (CA). Independent studies indicate that both CA activity and mesophyll conductance tend to scale with the photosynthetic capacity or the maximum carboxylation rate of Rubisco (Badger and Price, 1994; Evans et al., 1994), such that:

$$g_{COS} = \alpha * V_{cmax} \quad (4)$$

where  $\alpha$  is a parameter that is calibrated to observations of simultaneous measurements of COS and  $CO_2$  uptake (Stimler et al., 2012). Analysis of these measurements yield estimates of  $\alpha$  of  $\sim 1400$  for C3 and  $\sim 7500$  for C4 species (Stimler et al., 2012; Haynes et al., 2020). According to the COS modelling scheme of the Simple biosphere model (version 4.2) (Haynes et al., 2020),  $g_{COS}$  can be calculated as:

$$g_{COS} = 1.4 * 10^3 * (1.0 + 5.33 * F_{C4}) * 10^{-6} * F_{APAR} * f_w * V_{cmax} \quad (5)$$

where  $F_{C4}$  denotes the C4 plant flag, which takes the value of 1 when the vegetation is C4 plants and 0 otherwise.  $f_w$  is a soil moisture stress factor describing the sensitivity of  $g_{sw}$  to soil water availability (Ju et al., 2006).  $F_{APAR}$  is the scaling factor for leaf radiation, calculated as:

$$F_{APAR} = 1 - e^{(-0.45 * LAI)} \quad (6)$$

$F_{COS,soil}$  is taken as the combination of abiotic COS flux  $F_{cos,abiotic}$  and biotic COS flux  $F_{COS,biotic}$  (Whelan et al., 2016).

$$F_{COS,soil} = F_{COS,abiotic} + F_{COS,biotic} \quad (7)$$

$F_{COS,abiotic}$  is controlled by abiotic degradation of soil organic matter (Whelan and Rhew, 2015), can be described as an exponential function of the temperature of soil  $T_{soil}$  ( $^{\circ}C$ ).

$$F_{COS,abiotic} = e^{(\alpha + \beta * T_{soil})} \quad (8)$$

Where  $\alpha$  (unitless) and  $\beta$  ( $^{\circ}C^{-1}$ ) are parameters determined using the least-squares fitting approach.

$F_{COS,biotic}$  is attributed to CA in microbial communities (Sauze et al., 2017), calculated according to Behrendt et al. (2014) and Whelan et al. (2016):

$$F_{COS,biotic} = F_{opt} \left( \frac{SWC}{SWC_{opt}} \right) * e^{-a \left( \frac{SWC}{SWC_{opt}} - 1 \right)} \quad (9)$$

where  $a$  is the curve shape constant,  $SWC$  is the soil moisture (percent volumetric water content),  $F_{opt}$  denotes the optimal biotic COS uptake ( $pmol m^{-2} s^{-1}$ ) at optimum soil moisture  $SWC_{opt}$ . The curve shape constant  $a$  can be determined based on  $SWC_{opt}$ ,  $F_{opt}$ , and COS flux ( $F_g$ ) under another soil moisture condition ( $SWC_g$ , and  $SWC_g > SWC_{opt}$ ), as follows:

$$a = \ln \left( \frac{F_{opt}}{F_{SWC_g}} \right) * \left( \ln \left( \frac{SWC_{opt}}{SWC_g} \right) + \left( \frac{SWC_g}{SWC_{opt}} - 1 \right) \right)^{-1} \quad (10)$$

Here we use the parameterization scheme of soil COS modelling from Whelan et al. (2016) and Whelan et al. (2022), see **Table S2** and **Table S3** for details. Specifically, with reference to Abadie et al. (2022) and Whelan et al. (2022), the mean

195 modelled soil water content (SWC) and temperature of the top 9 cm of the soil profile in BEPS were utilized to drive the COS soil model in this study, and the mean modelled SWC and temperature were calculated through a weighted average considering the depth of each soil layer. A more detailed description about the soil hydrology and stomatal conductance modelling approach of BEPS is provided in the appendix.

## 2.2 Model parameters

200 NUCAS v1.0 can optimize 76 parameters belonging to BEPS. Of these parameters, some are global (i.e., the ratio of photosynthetically active radiation to shortwave radiation ( $f_{leaf}$ )), and others differentiated by PFT (i.e., maximum carboxylation rate of Rubisco at 25°C ( $V_{cmax25}$ )), or soil texture class (i.e.,  $Ksat_{scalar}$ , the scaling factor of saturated hydraulic conductivity (Ksat)). The prior values of the parameters are taken as model defaults which have been tuned in past model development and validation studies (Kattge et al., 2009; Chen et al., 2012). The prior uncertainty of parameters is set based on  
205 previous research, i.e., Ryu et al. (2018) and Chen et al. (2022). For a more detailed description of these parameters, see **Table S4** in the supplement.

## 2.3 Site description

In this study, NUCAS was operated at seven sites distributed over the Eurasian and North American continents characterized as boreal, temperate and subtropical regions (**Figure 2**) based on field observations collected from several studies. These sites  
210 were representative of different climate regions and land cover types (in the model represented by PFTs, and soil textures, as depicted in **Table 1**). They contained 4 of the 10 PFTs used in BEPS and 3 of the 11 soil textures. The sites comprise AT-Neu, located at an intensively managed temperate mountain grassland near the village of Neustift in the Stubai Valley, Austria (Hörtnagl et al., 2011; Spielmann et al., 2020); the Danish ICOS (Integrated Carbon Observation System) Research Infrastructure site (DK-Sor), which is dominated by European beech (Braendholt et al., 2018; Spielmann et al., 2019); the Las  
215 Majadas del Tietar site (ES-Lma) located in western Spain with a Mediterranean savanna ecosystem (El-Madany et al., 2018; Spielmann et al., 2019); the Hyytiälä forest Station (FI-Hyy), located in Finland and is dominated by Scots Pine (Bäck et al., 2012; Vesala et al., 2022); an agricultural soybean field measurement site (IT-Soy) located in Italy (Spielmann et al., 2019); the Harvard Forest Environmental Monitoring Site (US-Ha1) which is dominated by red oak and red maple in Petersham, Massachusetts, USA (Urbanski et al., 2007; Wehr et al., 2017); the Wind River Experimental Forest site (US-Wrc), located  
220 within the Gifford Pinchot National Forest in southwest Washington state, USA, with 478 ha of preserved old growth evergreen needleleaf forest (Rastogi et al., 2018). For further information on all sites, see publications listed in **Table 1**.

## 2.4 Data

NUCAS was driven by several temporally and spatially variant and invariant datasets. The CO<sub>2</sub> and COS mole fractions in the bulk air were assumed to be spatially invariant over the globe and to vary annually. The CO<sub>2</sub> mole fraction data in this study  
225 are taken from the Global Monitoring Laboratory (<https://gml.noaa.gov/ccgg/trends/global.html>). For the COS mole fraction, the average of the COS mole fraction observations from sites SPO (South Pole) and MLO (Mauna Loa, United States) were utilized to drive the model, the data are publicly available on line at: <https://gml.noaa.gov/hats/gases/OCS.html>. The other input data include a remotely sensed LAI dataset, a meteorological dataset and a soil dataset. Additionally, in order to conduct data assimilation experiments and to evaluate the effectiveness of the assimilation of COS fluxes, field observations including  
230 the ecosystem-scale (eddy-covariance or gradient-based) COS flux, GPP, sensible heat (H), evapotranspiration (ET), and SWC collected at the sites were used.

### 2.4.1 LAI dataset

The LAI dataset used here are the GLOBMAP global leaf area index product (Version 3) (see [GLOBMAP global Leaf Area Index since 1981 | Zenodo](#)), the Global Land Surface Satellite (GLASS) LAI product (Version 3) (acquired from <ftp://ftp.glcfc.umd.edu/>) and the level-4 MODIS global LAI product (see [LP DAAC - MOD15A2H \(usgs.gov\)](#)). The GLOBMAP LAI product quantifies leaf area index at a spatial resolution of 8×8 km and a temporal resolution of 8-day (Liu et al., 2012). The GLASS LAI product is generated every 8 days at a spatial resolution of 1×1 km (Xiao et al., 2016). And the MODIS LAI is an 8-day composite dataset with 500×500 m pixel size. As default, we used GLOBMAP products for assimilation experiments as much as possible given its good performance in the BEPS applications to various cases (Chen et al., 2019). The GLASS and MODIS LAI products were used to investigate the effect of the LAI products on the parameter optimization results. Also, according to Spielmann et al. (2019), the GLOBMAP product had considerably underestimated the LAI at the DK-Sor site in June 2016, and we noticed it was not consistent with the vegetation phenology at ES-Lma in May 2016. Therefore, GLASS LAI was used at these two sites and the GLOBMAP product was used at the remaining five sites. In addition, the 8-day temporal resolution of the LAI data was interpolated into daily values using the nearest neighbour method.

### 2.4.2 Meteorological dataset

Standard hourly meteorological data was inputted in BEPS, including air temperature at 2 m, shortwave radiation, precipitation, relative humidity and wind speed, taken from the FLUXNET database (for sites: AT-Neu, DK-Sor, ES-Lma, FI-Hyy and US-Ha1 see <https://fluxnet.org>), the AmeriFlux database (for sites: US-Ha1 and US-Wrc see <https://ameriflux.lbl.gov>) and the ERA5 dataset (for Sites: AT-Neu, IT-Soy, US-Ha1 see <https://cds.climate.copernicus.eu/cdsapp#!/dataset/reanalysis-era5-single-levels?tab=overview>), respectively. Since the experiments were conducted at the site scale, we used the FLUXNET and AmeriFlux data, which contains information about the downscaling of meteorological variables of the ERA-Interim reanalysis data product as far as possible, and supplemented them with ERA5 reanalysis data (Pastorello et al., 2020). Although AT-Neu is a FLUXNET site, its FLUXNET meteorological data are only available for the years 2002-2012 while the measurement of COS was performed in 2015. Therefore, we first performed a linear fit of its ERA5-Land data and FLUXNET meteorological data for 2002-2012, and then corrected the ERA5 data for 2015 with the fitted parameters to obtain downscaling information for the meteorological variables. Additionally, for US-Ha1, we used the FLUXNET data in 2012, and AmeriFlux data and ERA5 shortwave radiation data in 2013 to drive the BEPS model, due to the absence of FLUXNET data in 2013 and the lack of shortwave radiation data of AmeriFlux.

### 2.4.3 Assimilation and evaluation datasets

The hourly ecosystem-scale COS flux observations were used to perform data assimilation experiments and to evaluate the assimilation results. They were taken from existing studies (listed in **Table 1**) and were available for at least a month. Most of the ecosystem COS flux observations were obtained using the eddy-covariance (EC) technique, with the exception of US-Ha1 and US-Wrc, where the COS fluxes were derived with the gradient-based approach (Baldocchi, 2003; Wu et al., 2015; Kohonen et al., 2020). The COS soil flux measurements were collected using soil chamber, except at US-Ha1, where the gradient-based approach was used. Detailed information about the COS measurements can be found in the publications listed in **Table 1**. Specifically, only the measured ecosystem COS fluxes of FI-Hyy (Vesala et al., 2022) was utilized in this study. US-Wrc utilises the gradient-based approach to measure COS ecosystem flux (Rastogi et al., 2018), however available data is limited to only COS concentration measurements and lacking other parameters required, therefore this site risks introducing biases. Hence, a bias correction scheme was implemented to match the simulated and estimated the ecosystem-scale COS fluxes for US-Wrc. The objectives of this correction scheme are to obviate the need for accurate values of parameters relevant

for COS flux calculations, and to retain as much useful information from the COS concentration measurements as possible (Leung et al., 1999; Scholze et al., 2016). This was done by using the mean ( $\bar{M}$ ) and standard deviation ( $\sigma_M$ ) of the simulated COS flux to correct the COS flux observations ( $O$ ):

$$F = \frac{\sigma_M(O - \bar{O})}{\sigma_o} + \bar{M} \quad (11)$$

275 where  $\bar{O}$  and  $\sigma_o$  are mean and standard deviation of the observed COS flux series.  $F$  is the corrected observed COS flux, and the COS simulations were calculated using the prior parameters for the time period corresponding to the COS flux observations. The standard deviation of the ecosystem COS fluxes within 24 hours around each observation was calculated as an estimate of the observation uncertainty. For the case where there are no other observations within the surrounding 24 hours, the uncertainty was taken as the mean of the estimated uncertainties of the whole observation series.

280 Due to the coupling between leaf exchange of COS, CO<sub>2</sub> and H<sub>2</sub>O, GPP, and ET data are selected to evaluate the model performance of COS assimilation in this study. In addition, we further explored the ability of COS to constrain H simulations, since the transpiration contribute to a decrease in temperature within the leaf (Gates, 1968; Konarska et al., 2016), and the leaf-air temperature gradient is a key control factor of H (Monteith and Unsworth, 2013; Dong et al., 2017). Moreover, SWC is used in model evaluation as the key role of SWC in modelling  $F_{COS,biotic}$  (as shown in Eq. (9)) and that the water dissipated  
285 in transpiration originates from soil (Berry et al., 2006). A more detailed elaboration will be provided in the discussion.

These data were taken from FLUXNET (DK-Sor, ES-Lma, FI-Hyy and US-Ha1), AmeriFlux (US-Ha1 and US-Wrc), existing studies (Spielmann et al. (2020), Spielmann et al. (2019) and Rastogi et al. (2018)) and SMEAR (<https://smear.avaa.csc.fi/>). As only CO<sub>2</sub> turbulent flux (FC) data are available for US-Ha1 in 2013 and only net ecosystem exchange (NEE) data are  
290 available for IT-Soy, a night flux partitioning model was used to estimate ecosystem respiration ( $R_{eco}$ ) and thus to calculate GPP (Reichstein et al., 2005). The model assumes that nighttime NEE represents ecosystem respiration, and thus partitions FC or NEE into GPP and  $R_{eco}$  based on the semi-empirical models of respiration, which use air temperature as a driver (Lloyd and Taylor, 1994; Lasslop et al., 2012). While ET observations are only available at FI-Hyy from <https://smear.avaa.csc.fi/>, it can be derived from latent heat (LE), as the ratio of LE to the latent heat of vaporization ( $L_w$ ) (Pastorello et al., 2020). In this study, we use air temperature as a driver to calculated  $L_w$ , and subsequently ET (Bolton, 1980).

295 We hereby note that only the comparison of COS and GPP results before and after assimilation are presented in the main text, while the evaluation of the simulated ET (Figure S3 and S4), H (Figure S5 and S6), and SWC (Figure S7) are included in the supplement.

## 2.5 Experimental design

Three groups of data assimilation experiments were conducted in this study: (1) 14 model-based twin experiments were  
300 performed to investigate the ability of NUCAS to assimilate COS fluxes in different scenarios; (2) 13 single-site assimilation experiments were conducted at all seven sites to obtain the site-specific posterior parameters and the corresponding posterior model outputs based on COS flux observations; (3) one two-site assimilation experiment was carried out to refine one set of parameters over two sites simultaneously and to simulate the corresponding model outputs. Prior simulations using default parameters were also performed in order to investigate the effect of the COS flux assimilation. Moreover, due to the limitation  
305 of the COS observations, all of these experiments were conducted in a one-month time window at the peak of the growing season. Detailed information of these experiments is described in the following.



### 2.5.1 Twin experiment

Model-based twin experiments were performed to investigate the model performance of the data assimilation (Irrgang et al., 2017) at all seven sites considering single-site and two-site scenarios. In each twin experiment, we first created a pseudo-observation sequence by NUCAS using the prior parameters. The pseudo-observation time series included the prior simulated ecosystem COS fluxes with its uncertainties, and the latter were estimated as the standard deviation of the prior simulated COS fluxes within 24 hours around each simulation. Then, a given perturbation ratio was applied to the prior parameters vector, as a starting point for the interactive adjustment of parameter values to match the COS flux pseudo-observations. The effectiveness of the data assimilation methodology of NUCAS can be validated if it successfully restores the control parameters from the pseudo-observations. As a gradient-based optimization algorithm is used in NUCAS to tune the control parameters and minimize the cost function, the changes of cost function and gradient over assimilation processes can also be used to verify the assimilation performance of the system. In this work, a total of fourteen twin experiments were conducted, including thirteen single-site twin experiments and one two-site twin experiment. Regarding the uncertainty of parameters, a perturbation size of 0.2 was utilized in all of the twin experiments.

### 2.5.2 Real data assimilation experiment

After the ability of NUCAS to assimilate COS fluxes was confirmed by twin experiments, the system was then utilised to conduct data assimilation experiments with real COS observations under single-site and multi-site conditions to optimize the control parameters and state variables of this model, and use the evaluation dataset to test the posterior simulations of the state variables. For the single-site case, a total of thirteen data assimilation experiments were conducted at all sites to investigate the assimilation effect of COS flux on optimizing key ecosystem variables. Detailed information about those single-site experiments is shown in **Table 2**.

Single-site assimilation can fully account for the site-specific information, and thus achieve accurate calibration. However, this assimilation approach often yields a range of different model parameters between sites. For large-scale model simulations, only one set of accurate and generalized model parameters is required (Salmon et al., 2022). Thus, a two-site assimilation experiment, that can assimilate COS observations from two sites simultaneously, is necessary to be conducted. Although both DK-Sor and US-Ha1 are dominated by deciduous broadleaved forest, and both AT-Neu and ES-Lma are dominated by C3 grass, none of the COS flux observations from these two PFTs overlap in observation time. We therefore selected FI-Hyy and US-Wrc, which are both dominated by evergreen needleleaf forest, and conducted a two-site assimilation experiment with a one-month assimilation window in August 2014.

### 2.6 Model evaluation

For the purpose of demonstrating the process of control parameter vector being continuously adjusted in the normalized parameter space in a twin experiment, and quantifying the deviation of the current control vector from the prior, the distance ( $D_x$ ) between the parameter vector and the prior parameter vector was calculated.

$$D_x = \|x - x_0\| = \sqrt{\sum_{i=1}^n (x(i) - x_0(i))^2} \quad (12)$$

where  $i$  denotes the  $i$  th parameter in the parameter vectors and  $n$  denotes the number of parameters in the parameter vector, and takes a value of 76.

With the aim of evaluating the performance of NUCAS in the real data assimilation experiments, we reran the model to obtain the posterior model outputs based on the posterior model parameters. Typical statistical metrics including mean bias (MB),

345 root mean square error (RMSE) and coefficient of determination ( $R^2$ ) are used to measure the difference between the simulations and *in situ* observations. They were calculated as:

$$MB = \frac{1}{N} \sum_{i=1}^N (M_i - O_i) = \bar{M} - \bar{O} \quad (13)$$

$$RMSE = \sqrt{\frac{1}{N} \sum_{i=1}^N (M_i - O_i)^2} \quad (14)$$

$$R^2 = 1 - \frac{\sum_{i=1}^N (M_i - O_i)^2}{\sum_{i=1}^N (O_i - \bar{O})^2} \quad (15)$$

350 where  $M_i$  denotes the simulation corresponding to the  $i$  th observation  $O_i$  and  $N$  is the total number of observations. Additionally, in order to investigate the sensitivity of COS assimilation to the model parameters, we also calculated the sensitivity index (SI) for each parameter at the prior value based on the sensitivity information provided by the adjoint model. SI of  $i$  th parameter  $x(i)$  of the parameter vector  $x$  was calculated as:

$$SI(x(i)) = \frac{\partial J / \partial x(i)}{\|\partial J / \partial x\|} \quad (16)$$

355 where  $\|\partial J / \partial x\|$  denotes the norm of the sensitivity vector of the cost function to the model parameters.

### 3 Results

#### 3.1 Twin experiments

After averaging about 18 and 13 evaluations of the cost function and its gradients, each of the twin experiments was successfully performed. Details of those twin experiments are shown in **Table S5**. In summary, during those assimilations, the  
360 cost function values were substantially reduced by more than Thirteen orders of magnitude, from greater than 50.75 to less than  $5.09 \times 10^{-13}$  and the respective gradient values also reduced from greater than 38.81 to less than  $1.59 \times 10^{-6}$ , which verified the ability of the data assimilation algorithm to correctly complete the assimilation.

The relative changes of the parameters with respect to the prior values at the ends of the experiments, as well as the initial values ( $D_{initial}$ ) and the maximums ( $D_{max}$ ) and the final values ( $D_{final}$ ) of  $D_x$  are reported in **Table S5**. Results show that the  
365 relative differences of those parameters from the "true" values reached exceedingly small values at the ends of twin experiments, with the maximum of the absolute values of the relative changes below  $8.55 \times 10^{-9}$ .  $D_x$  was also reduced to nearly zero, where the maximum value was below  $6.60 \times 10^{-8}$ , which indicates that all parameters in the control parameter vectors were almost fully recovered from the pseudo-observations. In conclusion, these results demonstrate that NUCAS has excellent data assimilation capability under various scenarios with different perturbations, and can effectively perform iterative  
370 computations to obtain reliable parameter optimization.

#### 3.2 Single-site assimilation

With an average of approximately 92 cost function evaluations, all of the 13 single-site experiments were performed successfully. The experiments reduced cost function values substantially, with an average cost function reduction of 19.97% (**Table 2**). However, the cost function reduction of the experiment varies considerably with PFT, site and assimilation window,  
375 ranging from 2.84% to 63.73%. The cost function decreased dramatically at US-Ha1, with an average decrease of 53.93%. In contrast, at IT-Soy, the cost function reduction is only 4.87%. With a same PFT (C3 grass), the cost function decreased by a

similar degree at AT-Neu and ES-Lma, of 16.39% and 15.70%. The average cost function reduction at FI-Hyy (29.52%) was also comparable to another evergreen needleleaf forest site, US-Wrc (27.71%), in 2014. However, the cost function reduction of FI-Hyy varied notably from year to year. In July 2014 and August 2014, the cost function reductions were 20.17% and 38.86% respectively, while in July of all other years, the cost function reductions were much lower, ranging from 2.84% to 5.88%. Similar to the single-site twin experiments, only five parameters have been efficiently adjusted in the single site experiments (**Table 2**).

The mean diurnal cycle and the scatterplots of observed and simulated COS fluxes are presented in **Figure 3** and **Figure S1**, respectively. On average across all sites, the prior simulated and observed ecosystem COS fluxes were remarkably close, with 20.60  $\text{pmol m}^{-2} \text{s}^{-1}$  and 20.04  $\text{pmol m}^{-2} \text{s}^{-1}$  respectively. However, there was substantial variability between sites and even between experiments at the same site. At ES-Lma, the prior simulated COS fluxes were greatly underestimated by 63.38%. In contrast, the prior simulated COS fluxes were overestimated at US-Ha1, with MBs of -10.01  $\text{pmol m}^{-2} \text{s}^{-1}$  and -12.17  $\text{pmol m}^{-2} \text{s}^{-1}$  in July 2012 and July 2013. In general, the MBs of COS fluxes are largely determined by the simulations and observations at daytime due to the larger magnitude (**Figure 3**). However, the model-observation differences at nighttime are also non-negligible. As shown in **Figure 3**, the underestimation is particularly evident at AT-Neu, ES-Lma and FI-Hyy.

After the single-site optimizations, both the daily variation and diurnal cycle of COS simulations were improved. This was reflected in the reduction of mean RMSE between the simulated and the observed COS fluxes from 15.71  $\text{pmol m}^{-2} \text{s}^{-1}$  in the prior case to 13.84  $\text{pmol m}^{-2} \text{s}^{-1}$  in the posterior case. The RMSEs were also reduced in all single-site experiments. Moreover, the assimilation of COS fluxes also effectively corrected the bias between prior simulations and observations, with mean absolute MB decreased from 5.06 to 3.08  $\text{pmol m}^{-2} \text{s}^{-1}$ . In contrast,  $R^2$  remained almost unchanged by the optimizations, with its mean value of 0.30 in both the prior and posterior cases. Our results also showcase that the model-observation differences of COS fluxes were effectively reduced at daytime. However, the remarkable differences between COS flux observations and simulations at nighttime, are not effectively corrected in a number of assimilation experiments (i.e., the experiment conducted at FI-Hyy in July 2013, see **Figure 3d**).

### 3.3 Two-site assimilation

FI-Hyy and US-Wrc have different soil textures; sandy loam and loam, respectively. In the two-site assimilation experiment, NUCAS accounted for this difference appropriately and successfully minimized the cost function from 499.56 to 358.81 after 70 evaluations of cost function. The cost function reduction for the experiment has a value of 28.17%, comparable to the cost function reductions for corresponding single-site assimilation experiments at FI-Hyy and US-Wrc (38.86% and 27.71%). Furthermore, corresponding to these two soil textures, the texture-dependent parameters  $Ksat_{scalar}$  and  $b_{scalar}$  yielded two different posterior parameter values, respectively, so that a total of seven parameters were optimized in the two-site experiment (**Table 3**). It can be seen that the two-site optimized results of  $V_{cmax25}$ ,  $VJ_{slope}$  and  $f_{leaf}$  are similar to that of the single-site optimized results at US-Wrc, as most of the observations of the two-site experiment originated from US-Wrc. As for the texture-dependent parameters, they had the same signs and comparable magnitudes of the adjustments to that of the corresponding single-site experiment at FI-Hyy and were minutely adjusted at US-Wrc as in the corresponding single-site experiment. Overall, both the cost function reduction and the parameter optimization results of the two-site assimilation experiments were similar to the corresponding single-site experiments, demonstrating the ability of NUCAS to correctly perform joint data assimilation from COS observations at two sites simultaneously.

The posterior simulations of COS flux using the two-site posterior parameters, also demonstrated the ability of NUCAS to correctly assimilate two-site COS fluxes simultaneously (**Figure 3** and **Figure S1**). As shown in **Figure 3f** and **Figure 3m**, the prior COS simulations for both the FI-Hyy site and US-Wrc site were overestimated in the daytime compared to the

observations. After the two-site COS assimilation, the discrepancies between COS simulations and observations were reduced in both FI-Hyy and US-Wrc, with RMSE reductions of 18.42% and 3.23%, achieving similar results to the simulations using the single-site posterior parameters.

### 420 3.4 Parameter change

There were five parameters that have been adjusted during the assimilation of COS flux observations by NUCAS, whether in twin, single-site or two-site experiments. They are the maximum carboxylation rate at 25 °C ( $V_{cmax25}$ ), the ratio of  $V_{cmax}$  to maximum electron transport rate  $J_{max}$  (VJ\_slope), the scaling factor ( $Ksat_{scalar}$  and  $b_{scalar}$ ) of saturated hydraulic conductivity (Ksat) and Campbell parameter (b), and the ratio of PAR to shortwave radiation (f\_leaf). These parameters are  
425 strongly linked to the COS exchange processes and it is therefore reasonable that they could be optimized by the assimilation of COS flux. Furthermore, these parameters are also closely linked to processes such as photosynthesis, transpiration and soil water transport, and therefore the assimilation of COS flux provides an indirect constraint for improving the simulation of GPP, LE, H and soil moisture based on the assimilation of COS flux.

In both single-site and the two-site experiments,  $V_{cmax25}$  has been considerably adjusted, with average absolute relative change  
430 of 42.08% and 41.74%, respectively (**Figure 4a**). VJ\_slope and  $b_{scalar}$  also varied greatly in the single-site experiments, with mean absolute relative changes of 30.67% and 25.55%, respectively. However, in the two-site experiment, their mean absolute changes were much smaller, at 3.36% and 4.16%. The relative changes of  $Ksat_{scalar}$  are modest in both single-site and two-site experiments, with mean absolute values of 10.61% and 7.24%, respectively. As for f\_leaf, the average absolute relative changes are even smaller than that of  $Ksat_{scalar}$ , at 3.67% and 6.81% in the single-site and the two-site experiments.  
435 In addition, we found that the parameters can be tuned considerably in cases where the prior simulations are close to the observations. For example, at IT-Soy, where the prior simulations agree well with the observations and the cost function only decrease 4.87% in the experiment, both  $V_{cmax25}$  and  $b_{scalar}$  were remarkably tuned, with relative change of 32.55% and -44.72%.

Across all single-site experiments, there are notable differences in the results of parameter optimization, especially in  $V_{cmax25}$ .  
440 For the single-site experiment at US-Ha1 in July 2013, the posterior value of  $V_{cmax25}$  is 55.28% lower than the prior. In contrast, the posterior  $V_{cmax25}$  is 127.80% higher than the prior at ES-Lma. In addition to  $V_{cmax25}$ , the relative changes of  $b_{scalar}$  and VJ\_slope also vary considerably, ranging from -78.13% to 16.84% and -65.70% to 35.18%, respectively. On the contrary, the posterior values of f\_leaf show less variability, and do not differ from the prior value by more than 10.05% (note the difference in x-axis scales).

### 445 3.5 Parameter sensitivity

The adjoint-based sensitivity analysis results of the parameters are illustrated in **Figure 4b**. Our results suggest that  $V_{cmax25}$  has a critical impact on the assimilation results, followed by VJ\_slope. With absolute SIs ranging from 87.76% to 96.41%, the mean absolute SI of  $V_{cmax25}$  is about three times that of VJ\_slope, which are 29.71%. In contrast, the average absolute SIs of  $b_{scalar}$ , f\_leaf and  $Ksat_{scalar}$  are much lower, with 11.54%, 8.95% and 3.05% respectively.

450 Unlike the great variability of the posterior  $V_{cmax25}$  and VJ\_slope, the SIs of these two parameters are stable, especially at the same site. At US-Ha1, for example, the difference between the SIs of  $V_{cmax25}$  and VJ\_slope in its two experiments were all smaller than 3.05%. Furthermore,  $V_{cmax25}$  has the smallest magnitude of variation in SIs among the five parameters with the standard deviation of the SIs of 2.62%, despite its SIs are of a much larger order of magnitude. With the SIs ranging from 12.05% to 45.71% and 0.94% to 14.43%, VJ\_slope and f\_leaf also play important roles in the modelling of COS. As for  
455  $Ksat_{scalar}$  and  $b_{scalar}$ , their SIs varied considerably across sites and even across experiments at the same site. For example,

the absolute SIs of  $b_{scalar}$  are as high as 30.80% and 34.04% at the C3 grass sites AT-Neu and ES-Lma, respectively. On the contrary, the mean absolute SI of  $b_{scalar}$  is only 2.59% at FI-Hyy. Yet, the absolute SIs of  $b_{scalar}$  of FI-Hyy varies considerably across the experiments, ranging from 0.06% to 10.46%.

Our results also suggest that  $f_{leaf}$  tends to play a more important role in the COS assimilation at the forest sites (except  
460 DK-Sor, including FI-Hyy, US-Ha1 and US-Wrc) compared to the low-stature vegetation type sites (AT-Neu, ES-Lma and IT-Soy), with the mean absolute SIs about two times than that of the latter. With a mean absolute SI of 93.44%,  $V_{cmax25}$  is also observed to be more sensitive at the forest sites. Specifically, the largest SI of  $V_{cmax25}$  was observed at DK-Sor, while the SIs of  $VJ_{slope}$  and  $f_{leaf}$  of DK-Sor are noticeably lower than that of other sites, at 12.05% and 0.94%, respectively.

### 3.6 Comparison and evaluation of simulated GPP

465 For single-site experiments, both the prior and posterior GPP simulations performed well in modelling the daily variation and diurnal cycle of GPP, with mean  $R^2$  of 0.83 and 0.81, respectively (**Figure 5** and **Figure S2**). The discrepancy between simulations and observations was substantially reduced by the assimilation of COS, from mean RMSE of  $6.71 \text{ umol m}^{-2} \text{ s}^{-1}$  in the prior case to  $5.02 \text{ umol m}^{-2} \text{ s}^{-1}$  in the posterior case. Similar to COS, the mean of prior simulated GPP is also generally larger than the observed. With the assimilation of COS, the bias between the observed and simulated GPP was effectively  
470 corrected, with the reduction in mean absolute MB from  $3.83 \text{ umol m}^{-2} \text{ s}^{-1}$  to  $2.46 \text{ umol m}^{-2} \text{ s}^{-1}$ .

In general, the GPP performance was improved for most of the single-site experiments (12 of 13), with RMSE reductions ranging from 3.81% to 58.56%. Across all single-site experiments performed at evergreen needleleaf forest sites, the posterior GPP simulations were remarkably improved, with an averaged RMSE reduction of 37.05%. At the deciduous broadleaf forest sites (DK-Sor and US-Ha1), the posterior simulated GPP also achieved a better fit with the GPP derived from EC observations,  
475 with an averaged RMSE reduction of 22.16%. However, for experiments conducted on low-stature vegetation types (including C3 grass and C3 crop), the assimilation of COS is less effective in constraining the modelled GPP. At ES-Lma and IT-Soy, the RMSEs of the posterior simulated GPP are slightly lower than the prior, with reduction ratios of 8.60% and 3.81%, respectively. At AT-Neu, the addition of COS observation shifted the GPP simulations away from the GPP derived from EC observations, with the RMSE increasing from  $3.48 \text{ umol m}^{-2} \text{ s}^{-1}$  to  $5.97 \text{ umol m}^{-2} \text{ s}^{-1}$  (**Figure 5a**).

480 Covering different years or months, the single-site experiments performed at FI-Hyy and US-Ha1 provided an opportunity to analyze inter-annual and seasonal variation in the simulated and observed GPP. At US-Ha1, the prior simulations overestimated GPP in both July 2012 and July 2013, by 21.26% and 38.41% respectively. With the assimilation of COS, the modelled COS exhibited substantial decreases. In parallel, the model-observation difference of GPP also reduced, by 12.36% and 28.10%, respectively. However, the posterior simulated GPP appeared to be underestimated by 20.08%. At FI-Hyy, a total  
485 of six single-site experiments were conducted between 2013 and 2017, five of them in July and one in August 2014. The observed GPP shows little inter-annual variation in July from 2013 to 2017, with the mean ranging from  $8.30$  to  $9.15 \text{ umol m}^{-2} \text{ s}^{-1}$ . In August 2014, the GPP observations were noticeably lower than that in July, with a mean of  $6.43 \text{ umol m}^{-2} \text{ s}^{-1}$ . As for simulations, the model tends to overestimate GPP, with MBs ranging from  $2.24$  to  $3.59 \text{ umol m}^{-2} \text{ s}^{-1}$ . After the assimilation of COS, the overestimation of the COS simulation for FI-Hyy were effectively corrected, with the mean  
490 absolute MBs of  $1.53 \text{ umol m}^{-2} \text{ s}^{-1}$ . However, with a low SWC in August 2014, the prior simulated COS were obviously overestimated by 37.04%, which led to remarkable downward adjustments of  $V_{cmax25}$  as well as  $VJ_{slope}$ . Thus, the simulated GPP were also markedly downgraded by 55.38% in August 2014, ultimately resulting in the underestimation of the single-site posterior simulated GPP (**Figure 5f**).

In the two-site experiment, the model-observation differences of GPP for both FI-Hyy and US-Wrc were reduced by the  
495 assimilation of COS (**Figure 5f** and **Figure 5m**), with RMSE reductions of 42.96% and 43.11%, respectively. These RMSE

reductions are even higher than those in the corresponding single-site experiments, by 35.21% for FI-Hyy and 0.13% for US-Wrc. These results suggest that simultaneous assimilation using COS observations from two sites can also improve GPP simulations, and the assimilation can be more robust than the single-site assimilation because the possibility of over-fit local noise is reduced.

500 Overall, the assimilation of ecosystem COS fluxes improved the simulation of GPP in both single-site experiments and the two-site experiment. However, the assimilation effects vary considerably for different sites and even for different periods within the same site. Our results suggest the assimilation of COS is able to provide strong constrain to the modelling of GPP at forest sites, with an average RMSE reduction of 32.58%. In contrast, at the low-stature vegetation type (including C3 grass and C3 crop) sites, the assimilation of COS is less effective in constraining the GPP simulations.

## 505 4 Discussion

### 4.1 Parameter changes

As mentioned before, our results show  $V_{cmax25}$  was tuned the most in both the single-site experiments and the two-site experiments, with the mean absolute relative change of %, followed by VJ\_slope and  $b_{scalar}$ . This is because COS plant fluxes are much larger than COS fluxes of soil in general (Whelan et al., 2016; Whelan et al., 2018; Spielmann et al., 2019; Kooijmans et al., 2021; Ma et al., 2021; Maignan et al., 2021; Remaud et al., 2022) and the soil hydrology-related parameters cannot directly influence the COS plant uptake. Therefore, the assimilation of the COS flux mainly changed the parameters related to COS plant uptake rather than texture-dependent parameters that relate to soil COS flux to minimize the cost function. However, the adjustment of soil hydrology related parameters should not be neglected as well, as they play an important role in minimizing the discrepancy between COS simulations and observations.

515 As shown in **Figure 3**, the prior simulations underestimated COS fluxes at nighttime for many sites, i.e., FI-Hyy. On the one hand, this is due to the substantial gap between current modelled COS soil fluxes and observations (Whelan et al., 2022). On the other hand, this also stems from the fact that the nighttime stomatal conductance was set to a low and constant value ( $1 \text{ mmol m}^{-2} \text{ s}^{-1}$ ) in the BEPS model. As a result, the discrepancy between nighttime ecosystem COS simulations and observations could not be reduced by adjusting photosynthesis-related parameters to have an effect on stomatal conductance modelling. Thus, soil hydrology-related parameters were adjusted to compensate for the differences in both soil and plant components simultaneously. In this study, the COS soil model proposed by Whelan et al. (2016) and Whelan et al. (2022) was utilized, in which the optimal SWC for soil COS biotic uptake was set to 12.5 (%) for grass. Such an optimal SWC value is much lower than the prior simulated SWC, as shown in **Figure S7a** and **Figure S7c**. Therefore, the soil hydrology-related parameters were considerably tuned at AT-Neu and ES-Lma, resulting in a rapid decline in the posterior SWC simulation to a level comparable to the optimum SWC. COS plant uptake is governed by the hydrolysis reaction of COS (Wohlfahrt et al., 2012), catalysed by CA, though it can also be degraded by other photosynthetic enzymes, e.g., RuBisco (Lorimer and Pierce, 1989; Ma et al., 2021), and the reaction is not dependent on light (Stimler et al., 2011; Whelan et al., 2018). Yet, given that stomatal conductance is simulated from net photosynthetic rate with a modified version (Woodward et al., 1995; Ju et al., 2010) of the BB model (Ball et al., 1987) in BEPS, the adjustment of light reaction related parameters (VJ\_slope and  $f_{leaf}$ ) can therefore indirectly affect the simulation of COS plant uptake by influencing the calculation of stomatal conductance. According to Ryu et al. (2018),  $f_{leaf}$  varies little in reality and is usually between 41% and 53% on an annual mean scale. In our assimilation experiments, the optimized  $f_{leaf}$  values were distributed between 42.92% and 51.28%, consistent with this study. In contrast, the other light reaction related parameter VJ\_slope, has a much wider range of variation, with relative changes ranging from -65.70% to 35.18%.

535 We noticed remarkably different optimization results for photosynthesis-related parameters in the experiments conducted in July 2013 and July 2014 at FI-Hyy, especially for  $V_{cmax25}$  and VJ\_slope. In these two experiments, the difference in the relative change in both  $V_{cmax25}$  and VJ\_slope is more than 39%. However, these different adjustments to the parameter set caused similar impact on COS simulations, leading to the latter being reduced by 13.38% and 24.22% in July 2013 and July 2014, respectively. These results revealed the ‘equifinality’ (Beven, 1993) of the inversion problem at hand, i.e. the fact that different combinations of parameter values can achieve a similar fit to the COS observations. Assimilation of further observational data streams is expected to reduce the level of equifinality by differentiating between such combinations of parameter values that achieve a similar fit to COS observations.

#### 4.2 Parameter sensitivity

It has been proven that photosynthetic capacity simulated by terrestrial ecosystem models is highly sensitive to  $V_{cmax}$ ,  $J_{max}$ , and light conditions (Zaehle et al., 2005; Bonan et al., 2011; Rogers, 2014; Sargsyan et al., 2014; Koffi et al., 2015; Rogers et al., 2017). Therefore, it is expected that  $V_{cmax25}$ , VJ\_slope, and f\_leaf would markedly affect the optimization results, as these parameters ultimately have an impact on the simulation of plant COS uptake by influencing the estimation of photosynthesis capacity and stomatal conductance. Specifically, results of Wang et al. (2004), Verbeeck et al. (2006), Staudt et al. (2010), Han et al. (2020) and Ma et al. (2022) showed that the simulated photosynthetic capacity was generally more sensitive to  $J_{max}$  and light conditions than to  $V_{cmax}$ . However, due to the differences in the physiological mechanisms of COS plant uptake and photosynthesis, e.g., the hydrolysis reaction of COS by CA is not dependent on light, the sensitivities of the two processes with respect to the model parameters may differ considerably although they are tightly coupled. Indeed, our adjoint sensitivity results suggest that the same change of  $V_{cmax25}$  is capable of influencing the assimilation results to a greater extent than of VJ\_slope and f\_leaf. This result can be attributed to the model structure that  $V_{cmax25}$  not only affects the estimation of stomatal conductance through photosynthesis, but is also used to characterize mesophyll conductance and CA activity due to their linear relationships with  $V_{cmax}$  (Badger and Price, 1994; Evans et al., 1994; Berry et al., 2013). In addition, such a large sensitivity in  $V_{cmax25}$  also indicates the importance of accurate modelling of the apparent conductance of COS for ecosystem COS flux simulation.

As for  $Ksat_{scalar}$  and  $b_{scalar}$ , they also play an important role in the assimilation of COS since the SWC simulations of BEPS are sensitive to Ksat and b (Liu et al., 2011), and SWC is the primary factor for COS soil biotic flux modelling (Whelan et al., 2016). However, as the soil COS exchange is generally much smaller than COS plant uptake (Whelan et al., 2018) and the parameter scheme provided by Whelan et al. (2022) sets different empirical parameter values (See **Table S3** for details) depending on the PFTs, the SIs of  $Ksat_{scalar}$  and  $b_{scalar}$  differs considerably across PFTs, and are overall lower than those of photosynthesis related parameters.

565 In Sect 3.5, we mentioned that the radiation related parameter f\_leaf tend to play more essential roles in the assimilation of COS at the forest sites. Similar findings by Sun et al. (2019) found that the simulated GPP was more sensitive to radiation at forested vegetation types and less sensitive at low-stature vegetation types. Particularly, the simulated GPP was also found to be highly sensitive to variations of radiation at low radiation conditions (Koffi et al., 2015).

#### 4.3 Impacts of COS assimilation on ecosystem carbon, energy and water cycles

570 Due to the physiological basis that COS is taken up by plants through the same pathway of stomatal diffusion as  $CO_2$ , the assimilation of COS was expected to optimize the simulation of GPP. It was confirmed by our single-site and the two-site experiments conducted in a variety of ecosystems, including evergreen needleleaf forest, deciduous broadleaf forest, C3 grass

and C3 crop. However, limited by many factors, such as the observation errors of the COS fluxes, the assimilation of COS does not always improve the simulation of GPP, i.e., at AT-Neu site.

575 Similar to the photosynthesis, the transpiration is also coupled with the COS plant uptake through stomatal conductance. But the difference is that after CO<sub>2</sub> is transported to the chloroplast surface, it continues its journey inside the chloroplast, and is eventually assimilated in the Calvin cycle (Wohlfahrt et al., 2012; Kohonen et al., 2022). Based on the BB model, photosynthesis-related parameters only indirectly influence the calculation of stomatal conductance through photosynthesis in our model. Thus, ET was not optimized as dramatically as GPP in the assimilation of COS. In comparison, the RMSEs of GPP  
580 simulations were reduced by an average of 23.54% as a result of assimilation of COS, % but reducing ET by only 16.68%. Moreover, as transpiration rate and leaf temperature change show a linear relationship (Kümmerlen et al., 1999; Prytz et al., 2003) and surface-air temperature difference is a key control factor for sensible heat fluxes (Campbell and Norman, 2000; Arya, 2001; Jiang et al., 2022), the optimization for transpiration can therefore improve the simulation of leaf temperature and consequently improve the simulation of sensible heat flux.

585 Driven by the difference in water potential between the atmosphere and the substomatal cavity (Manzoni et al., 2013), the water is taken up by the roots, flows through the xylem, and exits through the leaf stomata to the atmosphere in the soil-plant-atmosphere continuum via evapotranspiration (Daly et al., 2004). Thus, when plants transpire, the water potential next to the roots decreases, driving water from bulk soil towards roots (Carminati et al., 2010) and reducing soil moisture. Certainly, soil moisture dynamics are also influenced by soil evaporation and leakage during inter-storm periods under ideal  
590 conditions (Daly et al., 2004). However, studies have shown that transpiration represents 80 to 90 percent of terrestrial evapotranspiration (Jasechko et al., 2013) and evaporation is typically a small fraction of transpiration for well-vegetated ecosystems (Scholes and Walker, 1993; Daly et al., 2004). Based on current knowledge of leakage, for example the relationship between leakage and the behavior of hydraulic conductivity (Clapp and Hornberger, 1978), extremely small adjustments of  $K_{sat}$  and  $b$ , i.e., with relative changes of % 0.0057% for  $K_{sat}_{scalar}$  and -0.057% for  $b_{scalar}$  in July 2015 at FI-Hyy, hardly  
595 caused any change in leakage. Therefore, our results indicate that the assimilation of COS not only can markedly improve the modelling of stomatal conductance and transpiration, but it can also ultimately improve SWC predictions. However, our results also show that there are obvious discrepancies between the ecosystem COS flux simulations and observations, and that discrepancies cannot be effectively reduced by the adjustment by the photosynthesis related parameters duo to the simplification of BEPS for nighttime stomatal conductance modelling. As a result, it was also observed that the soil hydrology  
600 related parameters were drastically adjusted to minimize the discrepancy of COS simulations and observations, which instead biased the SWC simulations away from observations, for example, as shown in **Figure S7a** and **Figure S7c**.

#### 4.4 Impacts of leaf area index data on parameter optimization

As an essential input data of the BEPS model, LAI products have been demonstrated to be a source of uncertainty in the simulation of carbon and water fluxes (Liu et al., 2018). Therefore, it is necessary to investigate the influence of LAI on our  
605 parameter optimization results, as the LAI is directly related to the simulation of COS and the discrepancy between COS simulations and COS observations is an essential part of the cost function. Here we collected three widely used satellite-derived LAI products (GLOBMAP, GLASS and MODIS) and the means of *in situ* LAI during the growing seasons or during the COS measurement periods for these sites (see **Table 1**). These *in situ* LAI means were used to drive the BEPS model along with the other three satellite-derived LAI products, with the assumption that they are representative of the LAI values during the  
610 assimilation periods. The configurations of those assimilation experiments were the same as those listed in **Table 2**, so that a total of 52 single-site experiments were conducted. All experiments were successfully performed, and the results were shown in **Figure 7** and **Figure S8**.



We found that the posterior  $V_{cmax25}$  significantly correlated with the LAI ( $R^2 = 0.22$ ,  $P < 0.01$ ) whilst there was no apparent relationship between the optimization results of the other three parameters and the LAI. As mentioned before, the LAI is directly related to the simulation of COS and thus influences the optimal values of the parameters. Therefore, the correlations of LAI with these parameters reflects the robustness of the constraint abilities of COS assimilation with respect to them. These results suggest that the assimilation of COS is able to provide strong constraints on  $V_{cmax25}$ , while it constrains other parameters ( $VJ\_slope$ ,  $Ksat_{scalar}$ ,  $b_{scalar}$ ,  $f\_leaf$ ) weakly, although they also considerably changed by the assimilation. In conclusion, our results suggest that the uncertainty in satellite-derived LAI not only can exert large impacts on the modelling of water-carbon fluxes (Wang et al., 2021), but also is an important source of the uncertainty in the parameter optimization results when performing data assimilation experiments with ecosystem models driven by LAI.

#### 4.5 Caveats and implications

In general, we found that the assimilation of COS can improve the model performance for GPP, ET and H for both single-site assimilation and two-site assimilation. Nonetheless, there are currently limitations that affect the use of COS data for the optimization of parameters, processes and variables related to water-carbon cycling and energy exchange in terrestrial ecosystem models.

The assimilation of COS fluxes relies on the availability and quality of field observations. As both COS plant uptake and COS soil exchange are modelled within NUCAS and the data assimilation was performed at the ecosystem scale, a large number of accurate measurements of both COS soil flux and COS plant flux are essential for COS assimilation and model evaluation. However, at present, we face a serious lack of COS measurements (Brühl et al., 2012; Wohlfahrt et al., 2012). More laboratory and field measurements are needed for better understanding of mechanistic processes of COS. Besides, the existing COS fluxes were calculated based on different measurement methods and data processing steps, which poses considerable challenges for comparing COS flux measurements across sites. Particularly, as only raw COS concentrations were provided and a correction approach was employed, the estimated COS fluxes at US-Wrc may subject to considerable uncertainties. Standardization of measurement and processing techniques of COS is therefore urgently needed (Kohonen et al., 2020).

In this study, the prior uncertainty of observation was estimated by the standard deviation of ecosystem COS fluxes within 24 hours with the assumption of a normal distribution. However, Hollinger and Richardson (2005) suggested that flux measurement error more closely follows a double exponential than a normal distribution. Kohonen et al. (2020) showed that the overall uncertainty in the COS flux varies with the sign (uptake or release) as well as the magnitude of the COS flux. Furthermore, there is a lack of understanding of the prior uncertainty for certain model parameters, such as  $VJ\_slope$ , which makes the uncertainty estimates subject to potentially large errors. In conclusion, we should be more careful in considering the distribution and the magnitude of the prior uncertainty of observations and parameters.

The spatial and temporal variation in atmospheric COS concentrations has a considerable influence on the COS plant uptake (Ma et al., 2021) due to the linear relationship between the two (Stimler et al., 2010). The typical seasonal amplitude of atmospheric COS concentrations is  $\sim 100$ – $200$  parts per trillion (ppt) around an average of  $\sim 500$  ppt (Montzka et al., 2007; Kooijmans et al., 2021; Hu et al., 2021; Ma et al., 2021; Belviso et al., 2022). However, in NUCAS, COS mole fractions in the bulk air are currently assumed to be spatially invariant over the globe and to vary annually, which may introduce substantial errors into the parameter calibration. Kooijmans et al. (2021) has confirmed that modifying the COS mole fractions to vary spatially and temporally markedly improved the simulation of ecosystem COS flux. Thus, we suggest to take into account the variation in COS concentration and their interaction with surface COS fluxes at high spatial and temporal resolution in order to achieve better parameter calibration.

Currently, there are still uncertainties in the simulation of COS fluxes by BEPS, particularly for nighttime COS fluxes. As the nighttime COS plant uptake is driven by stomatal conductance (Kooijmans et al., 2021), nighttime COS fluxes can therefore be used to test the accuracy of the model settings for nighttime stomatal conductance ( $g_n$ ). In the BEPS model, a low and constant value ( $1 \text{ mmol m}^{-2} \text{ s}^{-1}$ ) of  $g_n$  was set for all PFTs. Our simulations of nighttime COS flux indicate that in BEPS,  $g_n$  is underestimated to different degrees for different sites. Similar findings by Resco De Dios et al. (2019), showed that the median  $g_n$  in the global dataset was  $40 \text{ mmol m}^{-2} \text{ s}^{-1}$ . Therefore, utilizing COS to directly optimize stomatal related parameters should be perused. Cho et al. (2023) has proven the effectiveness of optimizing the minimum stomatal conductance as well as other parameters by the assimilation of COS. As different enzymes have different physiological characteristics, Cho et al. (2023) proposed a new temperature function for the CA enzyme and showcase the considerable difference in temperature response of enzymatic activities of CA and RuBisCo, which provided valuable insights into the modelling and assimilation of COS. In addition, soil COS exchange is an important source of uncertainty in the use of COS as carbon-water cycle tracer since CA activity occurs in the soil as well (Kesselmeier et al., 1999; Smith et al., 1999; Ogée et al., 2016; Meredith et al., 2019). Kaisermann et al. (2018) showed that COS hydrolysis rates were linked to microbial C biomass, whilst COS production rates were linked to soil nitrogen content and mean annual precipitation (MAP). Interestingly, MAP was also suggested to be the best predictor of  $g_n$  by Yu et al. (2019), who found that plants in locations with lower rainfall conditions had higher  $g_n$ . Therefore, using the global microbial C biomass, soil nitrogen content and MAP datasets, the relationships between these variables, and the associated COS exchange processes, it is to be expected that a more accurate modelling of terrestrial ecosystem COS fluxes could be achieved, further increasing our understanding of the global COS budget and facilitate the assimilation of COS fluxes.

## 5 Conclusions

Over the past decades, considerable efforts have been made to obtain field observations of COS ecosystem fluxes and to describe empirically or mechanistically COS plant uptake and soil exchange, which offers the possibility of investigating the ability of assimilating ecosystem COS flux to optimize parameters and variables related to the water and carbon cycles and energy exchange. In this study, we introduced the NUCAS system, which has been developed based on the BEPS model and was designed to have the ability to assimilate ecosystem COS fluxes. In NUCAS, a resistance analog model of COS plant uptake and an empirical model of soil COS flux were embedded in the BEPS model to achieve the simulation of ecosystem COS flux, and a gradient-based 4D-Var data assimilation algorithm was implemented to optimize the internal parameters of BEPS.

Fourteen twin experiments, thirteen single-site experiments and one two-site experiment covering the period from 2012 to 2017, were conducted to investigate the capability of NUCAS to assimilate COS fluxes and optimize output parameters and variables. COS flux observations from a range of ecosystems were used, including four PFTs and three soil textures. Our results show that NUCAS has the ability to optimize parameter vectors, and the assimilation of COS can constrain parameters affecting the simulation of carbon and water cycles and energy exchange and thus effectively improve the performance of the BEPS model. We found that there is a tight link between the assimilation of COS fluxes and the optimization of ET, which demonstrates the role of COS as an indicator of stomatal conductance and transpiration. The improvement of ET can further improve the model performance for H, although the propagation of the optimization effect is subject to some limitations. These results highlight the broad perspective of COS as a tracer for improving the simulation of variables related to stomatal conductance. Furthermore, we demonstrated that COS can provide a strong constraint on  $V_{cmax25}$ , whereas the adjustment of parameters related to the soil hydrology appears to compensate for weaknesses in the model, i.e., the nighttime stomatal conductance set in BEPS model. We also proved the strong impact of LAI on the parameter optimization results, emphasizing

the importance of developing more accurate LAI products for models driven by observed LAI. In addition, we made a number of recommendations for future improvement of the assimilation of COS. Particularly, we flagged the need for more observations of COS, suggested better characterisation of observational and prior parameter uncertainties, the use of varying  
695 COS concentrations and the refinement of the model for COS fluxes of soil. Specifically, with the lack of separate COS plant and soil flux data, the ecosystem-scale COS flux observations were utilized in this study. However, we believe that assimilating the component fluxes of COS individually should be pursued in the future as this assimilation approach would provide separate constraints on different parts of the model. We expect the observational information on the partitioning between the two flux components to provide a stronger constraint than using just their sum.

700 Our two-site setup constitutes a challenge for the assimilation system, the model and the observations. In this setup, the assimilation system has to determine a parameter set that achieves a fit to the observations at both sites, and NUCAS passes this important test. It should be noted that NUCAS was designed as a platform that integrates multiple data streams to provide a consistent map of the terrestrial carbon cycle although only ecosystem COS fluxes were used to evaluate the performance of NUCAS in this study. The “two-site” assimilation experiment conducted in this study gives us more confidence that the  
705 calibrated model will provide a reasonable parameter set and posterior simulation throughout the plant functional type. In other words, what we present here is a pre-requisite for applying the model and assimilation system at regional to global scales.

We noticed the optimization of model parameters faced the challenge of ‘equifinality’ due to the complexity of the model and the limited observation data. However, the ‘equifinality’ can be avoided by imposing additional observational constraints (Beven, 2006). Indeed, using several different data streams to simultaneously (Kaminski et al., 2012; Schürmann et al., 2016;  
710 Scholze et al., 2016; Wu et al., 2018; Scholze et al., 2019) or step-wise (Peylin et al., 2016) to constrain multiple processes in the carbon cycle is becoming a focus area in carbon cycle research. Therefore, it is necessary to combine COS with other observations to constrain different ecosystem processes and/or exploit multiple constraints on the same processes in order to achieve better modelling and prediction of the ecosystem water-carbon cycle and energy exchange.

715 *Code availability.* The source code for BEPS is publicly available at <https://zenodo.org/doi/10.5281/zenodo.8288750>, the adjoint code for BEPS is available upon request to the correspondence author (mousongwu@nju.edu.cn).

*Data availability.* Measured eddy covariance Carboy sulfide fluxes data can be found at <https://zenodo.org/records/3993111> for AT-Neu, <https://zenodo.org/record/3406990> for DK-Sor, ES-Lma and IT-Soy, <https://zenodo.org/record/6940750> for  
720 FI-Hyy, and from the Harvard Forest Data Archive under record HF214 (<https://portal.edirepository.org/nis/mapbrowse?packageid=knb-lter-hfr.214.4>) for US-Ha1. The raw COS concentration data of US-Wrc can be obtained at <https://zenodo.org/record/1422820>. The meteorological data can be obtained from the FLUXNET database (<https://fluxnet.org/>) for AT-Neu, DK-Sor, ES-Lma, FI-Hyy and US-Ha1; from the AmeriFlux database (<https://ameriflux.lbl.gov/>) for US-Ha1 (except shortwave radiation data) and US-Wrc; from the ERA5 dataset  
725 (<https://cds.climate.copernicus.eu/cdsapp#!/dataset/reanalysis-era5-single-levels?tab=overview>) for AT-Neu, IT-Soy and US-Ha1. The evaluation data can be obtained from the FLUXNET database for DK-Sor, ES-Lma, FI-Hyy and US-Ha1; from the AmeriFlux database for US-Ha1 and US-Wrc; from <https://zenodo.org/records/3993111> for AT-Neu, from <https://smear.avaa.csc.fi/> for FI-Hyy, from <https://zenodo.org/record/6940750> for IT-Soy and from <https://zenodo.org/record/1422820> for US-Wrc. The H and LE data of AT-Neu and IT-Soy are provided by Felix M. Spielmann  
730 and Georg Wohlfahrt. The GLOBMAP LAI is available at <https://zenodo.org/record/4700264#.YzvSYnZBxD8%2F>, the GLASS LAI is available at <ftp://ftp.glcf.umd.edu/>, and the MODIS LAI product is available at

<https://lpdaac.usgs.gov/products/mod15a2hv006/>. All datasets used in this study and the model outputs are available upon request.

735 *Author contributions:* MW designed the experiments and developed the model, MV and TK developed the data assimilation layer including the adjoint code for the ecosystem model, HZ wrote the original manuscript and made the analysis. All the authors contributed to the writing of the manuscript.

*Competing interests:* The authors declare that they have no conflict of interest.

740

*Acknowledgements:* This study was supported by the National Key Research and Development Program of China (2023YFB3907402), the National Natural Science Foundation of China (42371486), the Research Funds for the Frontiers Science Center for Critical Earth Material Cycling, Nanjing University (Grant No: 0209-14380115, 0904-14380031). We thank Felix M. Spielmann and Georg Wohlfahrt for providing H and LE data for AT-Neu and IT-Soy. MV and TK thank

745 Laurent Hascoët for supporting this activity. The authors thank two anonymous reviewers for highly valuable comments.

## References

- Abadie, C., Maignan, F., Remaud, M., Ogée, J., Campbell, J. E., Whelan, M. E., Kitz, F., Spielmann, F. M., Wohlfahrt, G., and Wehr, R.: Global modelling of soil carbonyl sulfide exchanges, *Biogeosciences*, 19, 2427-2463, 2022.
- An, X. Q., Zhai, S. X., Jin, M., Gong, S., and Wang, Y.: Development of an adjoint model of GRAPES-CUACE and its application in tracking influential haze source areas in north China, *Geoscientific Model Development*, 9, 2153-2165, 2016.
- 750 Arias, P., Bellouin, N., Coppola, E., Jones, R., Krinner, G., Marotzke, J., Naik, V., Palmer, M., Plattner, G.-K., and Rogelj, J.: Climate Change 2021: The Physical Science Basis. Contribution of Working Group I to the Sixth Assessment Report of the Intergovernmental Panel on Climate Change; Technical Summary, 2021.
- Arya, P. S.: Introduction to micrometeorology, Elsevier2001.
- 755 Asaf, D., Rotenberg, E., Tatarinov, F., Dicken, U., Montzka, S. A., and Yakir, D.: Ecosystem photosynthesis inferred from measurements of carbonyl sulphide flux, *Nature Geoscience*, 6, 186-190, 2013.
- Bäck, J., Aalto, J., Henriksson, M., Hakola, H., He, Q., and Boy, M.: Chemodiversity of a Scots pine stand and implications for terpene air concentrations, *Biogeosciences*, 9, 689-702, 2012.
- Badger, M. R. and Price, G. D.: The role of carbonic anhydrase in photosynthesis, *Annual review of plant biology*, 45, 369-392, 1994.
- 760 Baldocchi, D. D.: Assessing the eddy covariance technique for evaluating carbon dioxide exchange rates of ecosystems: past, present and future, *Global change biology*, 9, 479-492, 2003.
- Ball, J. T., Woodrow, I. E., and Berry, J. A.: A model predicting stomatal conductance and its contribution to the control of photosynthesis under different environmental conditions, *Progress in photosynthesis research: volume 4 proceedings of the VIIth international congress on photosynthesis providence, Rhode Island, USA, august 10–15, 1986*, 221-224,
- 765 Behrendt, T., Veres, P. R., Ashuri, F., Song, G., Flanz, M., Mamtimin, B., Bruse, M., Williams, J., and Meixner, F. X.: Characterisation of NO production and consumption: new insights by an improved laboratory dynamic chamber technique, *Biogeosciences*, 11, 5463-5492, 10.5194/bg-11-5463-2014, 2014.
- Belviso, S., Remaud, M., Abadie, C., Maignan, F., Ramonet, M., and Peylin, P.: Ongoing Decline in the Atmospheric COS Seasonal Cycle Amplitude over Western Europe: Implications for Surface Fluxes, *Atmosphere*, 13, 812, 2022.
- 770 Berry, J., Wolf, A., Campbell, J. E., Baker, I., Blake, N., Blake, D., Denning, A. S., Kawa, S. R., Montzka, S. A., and Seibt, U.: A coupled model of the global cycles of carbonyl sulfide and CO<sub>2</sub>: A possible new window on the carbon cycle, *Journal of Geophysical Research: Biogeosciences*, 118, 842-852, 2013.
- Berry, S. L., Farquhar, G. D., and Roderick, M. L.: Co - evolution of climate, soil and vegetation, *Encyclopedia of hydrological sciences*, 2006.
- 775 Beven, K.: Prophecy, reality and uncertainty in distributed hydrological modelling, *Advances in water resources*, 16, 41-51, 1993.
- Beven, K.: A manifesto for the equifinality thesis, *Journal of hydrology*, 320, 18-36, 2006.
- Bolton, D.: The computation of equivalent potential temperature, *Monthly weather review*, 108, 1046-1053, 1980.
- 780 Bonan, G. B.: A biophysical surface energy budget analysis of soil temperature in the boreal forests of interior Alaska, *Water Resources Research*, 27, 767-781, 1991.

- Bonan, G. B., Lawrence, P. J., Oleson, K. W., Levis, S., Jung, M., Reichstein, M., Lawrence, D. M., and Swenson, S. C.: Improving canopy processes in the Community Land Model version 4 (CLM4) using global flux fields empirically inferred from FLUXNET data, *Journal of Geophysical Research: Biogeosciences*, 116, 2011.
- 785 Braendholt, A., Ibrom, A., Larsen, K. S., and Pilegaard, K.: Partitioning of ecosystem respiration in a beech forest, *Agricultural and Forest Meteorology*, 252, 88-98, 2018.
- Brühl, C., Lelieveld, J., Crutzen, P., and Tost, H.: The role of carbonyl sulphide as a source of stratospheric sulphate aerosol and its impact on climate, *Atmospheric Chemistry and Physics*, 12, 1239-1253, 2012.
- Campbell, G. S. and Norman, J. M.: *An introduction to environmental biophysics*, Springer Science & Business Media 2000.
- 790 Campbell, J. E., Carmichael, G. R., Chai, T., Mena-Carrasco, M., Tang, Y., Blake, D., Blake, N., Vay, S. A., Collatz, G. J., and Baker, I.: Photosynthetic control of atmospheric carbonyl sulfide during the growing season, *Science*, 322, 1085-1088, 2008.
- Carminati, A., Moradi, A. B., Vetterlein, D., Vontobel, P., Lehmann, E., Weller, U., Vogel, H.-J., and Oswald, S. E.: Dynamics of soil water content in the rhizosphere, *Plant and soil*, 332, 163-176, 2010.
- 795 Chen, J., Liu, J., Cihlar, J., and Goulden, M.: Daily canopy photosynthesis model through temporal and spatial scaling for remote sensing applications, *Ecological modelling*, 124, 99-119, 1999.
- Chen, J. M., Ju, W., Ciais, P., Viovy, N., Liu, R., Liu, Y., and Lu, X.: Vegetation structural change since 1981 significantly enhanced the terrestrial carbon sink, *Nature communications*, 10, 4259, 2019.
- Chen, J. M., Mo, G., Pisek, J., Liu, J., Deng, F., Ishizawa, M., and Chan, D.: Effects of foliage clumping on the estimation of global terrestrial gross primary productivity, *Global Biogeochemical Cycles*, 26, 2012.
- 800 Chen, J. M., Wang, R., Liu, Y., He, L., Croft, H., Luo, X., Wang, H., Smith, N. G., Keenan, T. F., and Prentice, I. C.: Global datasets of leaf photosynthetic capacity for ecological and earth system research, *Earth System Science Data*, 14, 4077-4093, 2022.
- Cho, A., Kooijmans, L. M., Kohonen, K.-M., Wehr, R., and Krol, M. C.: Optimizing the carbonic anhydrase temperature response and stomatal conductance of carbonyl sulfide leaf uptake in the Simple Biosphere model (SiB4), *Biogeosciences*, 20, 2573-2594, 2023.
- 805 Clapp, R. B. and Hornberger, G. M.: Empirical equations for some soil hydraulic properties, *Water resources research*, 14, 601-604, 1978.
- Commane, R., Meredith, L. K., Baker, I. T., Berry, J. A., Munger, J. W., Montzka, S. A., Templer, P. H., Juice, S. M., Zahniser, M. S., and Wofsy, S. C.: Seasonal fluxes of carbonyl sulfide in a midlatitude forest, *Proceedings of the National Academy of Sciences*, 112, 14162-14167, 2015.
- Daly, E., Porporato, A., and Rodriguez-Iturbe, I.: Coupled dynamics of photosynthesis, transpiration, and soil water balance. Part I: Upscaling from hourly to daily level, *Journal of Hydrometeorology*, 5, 546-558, 2004.
- Deng, F., Jones, D., Henze, D., Bousserrez, N., Bowman, K., Fisher, J., Nassar, R., O'Dell, C., Wunch, D., and Wennberg, P.: 815 Inferring regional sources and sinks of atmospheric CO<sub>2</sub> from GOSAT XCO<sub>2</sub> data, *Atmospheric Chemistry and Physics*, 14, 3703-3727, 2014.
- Dong, N., Prentice, I., Harrison, S. P., Song, Q., and Zhang, Y.: Biophysical homeostasis of leaf temperature: A neglected process for vegetation and land - surface modelling, *Global Ecology and Biogeography*, 26, 998-1007, 2017.
- Dowd, M.: Bayesian statistical data assimilation for ecosystem models using Markov Chain Monte Carlo, *Journal of Marine Systems*, 68, 439-456, 2007.
- 820 El-Madany, T. S., Reichstein, M., Perez-Priego, O., Carrara, A., Moreno, G., Martín, M. P., Pacheco-Labrador, J., Wohlfahrt, G., Nieto, H., and Weber, U.: Drivers of spatio-temporal variability of carbon dioxide and energy fluxes in a Mediterranean savanna ecosystem, *Agricultural and Forest Meteorology*, 262, 258-278, 2018.
- Evans, J. R., Caemmerer, S., Setchell, B. A., and Hudson, G. S.: The relationship between CO<sub>2</sub> transfer conductance and leaf anatomy in transgenic tobacco with a reduced content of Rubisco, *Functional Plant Biology*, 21, 475-495, 1994.
- 825 Farquhar, G. D., von Caemmerer, S. v., and Berry, J. A.: A biochemical model of photosynthetic CO<sub>2</sub> assimilation in leaves of C<sub>3</sub> species, *planta*, 149, 78-90, 1980.
- Fisher, J. B., Huntzinger, D. N., Schwalm, C. R., and Sitch, S.: Modeling the terrestrial biosphere, *Annual Review of Environment and Resources*, 39, 91-123, 2014.
- 830 Fisher, R. A. and Koven, C. D.: Perspectives on the Future of Land Surface Models and the Challenges of Representing Complex Terrestrial Systems, *Journal of Advances in Modeling Earth Systems*, 12, e2018MS001453, 2020.
- Friedlingstein, P., Jones, M. W., O'Sullivan, M., Andrew, R. M., Bakker, D. C., Hauck, J., Le Quéré, C., Peters, G. P., Peters, W., and Pongratz, J.: Global carbon budget 2021, *Earth System Science Data*, 14, 1917-2005, 2022.
- Gates, D. M.: Transpiration and leaf temperature, *Annual Review of Plant Physiology*, 19, 211-238, 1968.
- 835 Goldan, P. D., Fall, R., Kuster, W. C., and Fehsenfeld, F. C.: Uptake of COS by growing vegetation: A major tropospheric sink, *Journal of Geophysical Research: Atmospheres*, 93, 14186-14192, 1988.
- Grimm, N. B., Chapin III, F. S., Bierwagen, B., Gonzalez, P., Groffman, P. M., Luo, Y., Melton, F., Nadelhoffer, K., Pairis, A., and Raymond, P. A.: The impacts of climate change on ecosystem structure and function, *Frontiers in Ecology and the Environment*, 11, 474-482, 2013.
- 840 Gu, L., Baldocchi, D., Verma, S. B., Black, T., Vesala, T., Falge, E. M., and Dowty, P. R.: Advantages of diffuse radiation for terrestrial ecosystem productivity, *Journal of Geophysical Research: Atmospheres*, 107, ACL 2-1-ACL 2-23, 2002.

- Han, T., Zhu, G., Ma, J., Wang, S., Zhang, K., Liu, X., Ma, T., Shang, S., and Huang, C.: Sensitivity analysis and estimation using a hierarchical Bayesian method for the parameters of the FvCB biochemical photosynthetic model, *Photosynthesis research*, 143, 45-66, 2020.
- 845 Hascoët, L. and Pascual, V.: The Tapenade automatic differentiation tool: Principles, model, and specification, *ACM Trans. Math. Softw.*, 39, Article 20, 10.1145/2450153.2450158, 2013.
- Haynes, K., Baker, I., and Denning, S.: Simple biosphere model version 4.2 (SiB4) technical description, Colorado State University: Fort Collins, CO, USA, 2020.
- 850 He, Q., Ju, W., Dai, S., He, W., Song, L., Wang, S., Li, X., and Mao, G.: Drought risk of global terrestrial gross primary productivity over the last 40 years detected by a remote sensing - driven process model, *Journal of Geophysical Research: Biogeosciences*, 126, e2020JG005944, 2021.
- Hollinger, D. and Richardson, A.: Uncertainty in eddy covariance measurements and its application to physiological models, *Tree physiology*, 25, 873-885, 2005.
- 855 Hörtnagl, L., Bamberger, I., Graus, M., Ruuskanen, T. M., Schnitzhofer, R., Müller, M., Hansel, A., and Wohlfahrt, G.: Biotic, abiotic, and management controls on methanol exchange above a temperate mountain grassland, *Journal of Geophysical Research: Biogeosciences*, 116, 2011.
- Hu, L., Montzka, S. A., Kaushik, A., Andrews, A. E., Sweeney, C., Miller, J., Baker, I. T., Denning, S., Campbell, E., and Shiga, Y. P.: COS-derived GPP relationships with temperature and light help explain high-latitude atmospheric CO<sub>2</sub> seasonal cycle amplification, *Proceedings of the National Academy of Sciences*, 118, e2103423118, 2021.
- 860 Irrgang, C., Saynisch, J., and Thomas, M.: Utilizing oceanic electromagnetic induction to constrain an ocean general circulation model: A data assimilation twin experiment, *Journal of Advances in Modeling Earth Systems*, 9, 1703-1720, 2017.
- Jasechko, S., Sharp, Z. D., Gibson, J. J., Birks, S. J., Yi, Y., and Fawcett, P. J.: Terrestrial water fluxes dominated by transpiration, *Nature*, 496, 347-350, 2013.
- 865 Jiang, K., Pan, Z., Pan, F., Wang, J., Han, G., Song, Y., Zhang, Z., Huang, N., Ma, S., and Chen, X.: Influence patterns of soil moisture change on surface-air temperature difference under different climatic background, *Science of the Total Environment*, 822, 153607, 2022.
- Ju, W., Gao, P., Wang, J., Zhou, Y., and Zhang, X.: Combining an ecological model with remote sensing and GIS techniques to monitor soil water content of croplands with a monsoon climate, *Agricultural Water Management*, 97, 1221-1231, 2010.
- 870 Ju, W., Chen, J. M., Black, T. A., Barr, A. G., Liu, J., and Chen, B.: Modelling multi-year coupled carbon and water fluxes in a boreal aspen forest, *Agricultural and Forest Meteorology*, 140, 136-151, 2006.
- Kaisermann, A., Ogée, J., Sauze, J., Wohl, S., Jones, S. P., Gutierrez, A., and Wingate, L.: Disentangling the rates of carbonyl sulfide (COS) production and consumption and their dependency on soil properties across biomes and land use types, *Atmospheric Chemistry and Physics*, 18, 9425-9440, 2018.
- 875 Kaminski, T., Knorr, W., Scholze, M., Gobron, N., Pinty, B., Giering, R., and Mathieu, P.-P.: Consistent assimilation of MERIS FAPAR and atmospheric CO<sub>2</sub> into a terrestrial vegetation model and interactive mission benefit analysis, *Biogeosciences*, 9, 3173-3184, 2012.
- Kato, T., Knorr, W., Scholze, M., Veenendaal, E., Kaminski, T., Kattge, J., and Gobron, N.: Simultaneous assimilation of satellite and eddy covariance data for improving terrestrial water and carbon simulations at a semi-arid woodland site in Botswana, *Biogeosciences*, 10, 789-802, 2013.
- 880 Kattge, J., Knorr, W., Raddatz, T., and Wirth, C.: Quantifying photosynthetic capacity and its relationship to leaf nitrogen content for global - scale terrestrial biosphere models, *Global Change Biology*, 15, 976-991, 2009.
- Keenan, T. F., Davidson, E., Moffat, A. M., Munger, W., and Richardson, A. D.: Using model - data fusion to interpret past trends, and quantify uncertainties in future projections, of terrestrial ecosystem carbon cycling, *Global Change Biology*, 18, 2555-2569, 2012.
- 885 Kesselmeier, J., Teusch, N., and Kuhn, U.: Controlling variables for the uptake of atmospheric carbonyl sulfide by soil, *Journal of Geophysical Research: Atmospheres*, 104, 11577-11584, 1999.
- Knorr, W. and Heimann, M.: Impact of drought stress and other factors on seasonal land biosphere CO<sub>2</sub> exchange studied through an atmospheric tracer transport model, *Tellus B*, 47, 471-489, 1995.
- 890 Knorr, W., Kaminski, T., Scholze, M., Gobron, N., Pinty, B., Giering, R., and Mathieu, P. P.: Carbon cycle data assimilation with a generic phenology model, *Journal of Geophysical Research: Biogeosciences*, 115, 2010.
- Koffi, E., Rayner, P., Norton, A., Frankenberg, C., and Scholze, M.: Investigating the usefulness of satellite-derived fluorescence data in inferring gross primary productivity within the carbon cycle data assimilation system, *Biogeosciences*, 12, 4067-4084, 2015.
- 895 Kohonen, K.-M., Kolari, P., Kooijmans, L. M., Chen, H., Seibt, U., Sun, W., and Mammarella, I.: Towards standardized processing of eddy covariance flux measurements of carbonyl sulfide, *Atmospheric Measurement Techniques*, 13, 3957-3975, 2020.
- Kohonen, K.-M., Dewar, R., Tramontana, G., Mauranen, A., Kolari, P., Kooijmans, L. M., Papale, D., Vesala, T., and Mammarella, I.: Intercomparison of methods to estimate gross primary production based on CO<sub>2</sub> and COS flux
- 900 measurements, *Biogeosciences*, 19, 4067-4088, 2022.
- Konarska, J., Uddling, J., Holmer, B., Lutz, M., Lindberg, F., Pleijel, H., and Thorsson, S.: Transpiration of urban trees and its cooling effect in a high latitude city, *International journal of biometeorology*, 60, 159-172, 2016.

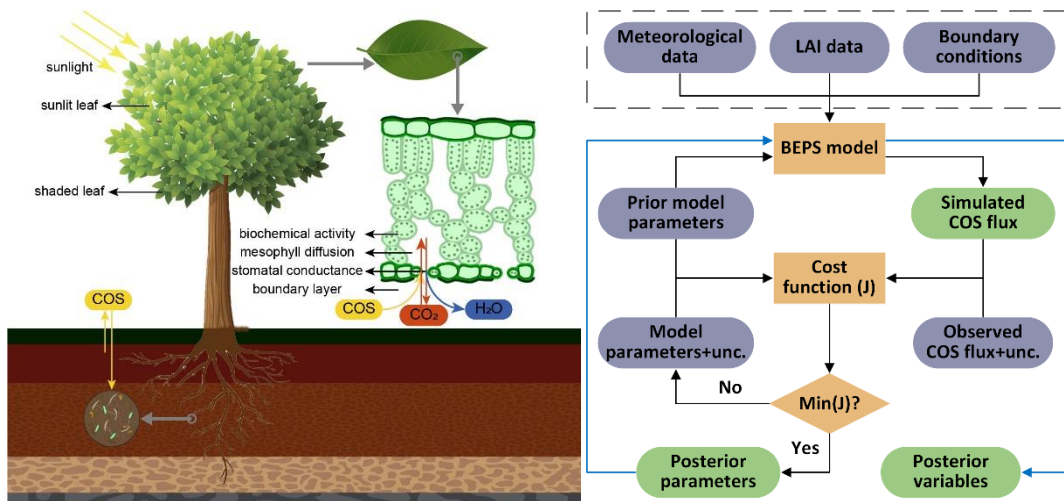
- Kooijmans, L. M., Sun, W., Aalto, J., Erkkilä, K.-M., Maseyk, K., Seibt, U., Vesala, T., Mammarella, I., and Chen, H.: Influences of light and humidity on carbonyl sulfide-based estimates of photosynthesis, *Proceedings of the National Academy of Sciences*, 116, 2470-2475, 2019.
- 905 Kooijmans, L. M. J., Cho, A., Ma, J., Kaushik, A., Haynes, K. D., Baker, I., Luijkx, I. T., Groenink, M., Peters, W., Miller, J. B., Berry, J. A., Ogée, J., Meredith, L. K., Sun, W., Kohonen, K. M., Vesala, T., Mammarella, I., Chen, H., Spielmann, F. M., Wohlfahrt, G., Berkelhammer, M., Whelan, M. E., Maseyk, K., Seibt, U., Commane, R., Wehr, R., and Krol, M.: Evaluation of carbonyl sulfide biosphere exchange in the Simple Biosphere Model (SiB4), *Biogeosciences*, 18, 6547-6565, 10.5194/bg-18-6547-2021, 2021.
- 910 Kümmerlen, B., Dauwe, S., Schmundt, D., and Schurr, U.: Thermography to measure water relations of plant leaves, *Handbook of computer vision and applications*, 3, 763-781, 1999.
- Lasslop, G., Migliavacca, M., Bohrer, G., Reichstein, M., Bahn, M., Ibrom, A., Jacobs, C., Kolari, P., Papale, D., and Vesala, T.: On the choice of the driving temperature for eddy-covariance carbon dioxide flux partitioning, *Biogeosciences*, 9, 5243-5259, 2012.
- 915 Launois, T., Peylin, P., Belviso, S., and Poulter, B.: A new model of the global biogeochemical cycle of carbonyl sulfide—Part 2: Use of carbonyl sulfide to constrain gross primary productivity in current vegetation models, *Atmospheric Chemistry and Physics*, 15, 9285-9312, 2015.
- Law, K., Stuart, A., and Zygalakis, K.: *Data assimilation*, Cham, Switzerland: Springer, 214, 52, 2015.
- 920 Leung, L. R., Hamlet, A. F., Lettenmaier, D. P., and Kumar, A.: Simulations of the ENSO hydroclimate signals in the Pacific Northwest Columbia River basin, *Bulletin of the American Meteorological Society*, 80, 2313-2330, 1999.
- Liu, J., Chen, J., and Cihlar, J.: Mapping evapotranspiration based on remote sensing: An application to Canada's landmass, *Water resources research*, 39, 2003.
- Liu, J., Chen, J., Cihlar, J., and Park, W.: A process-based boreal ecosystem productivity simulator using remote sensing inputs, *Remote sensing of environment*, 62, 158-175, 1997.
- 925 Liu, Y. and Gupta, H. V.: Uncertainty in hydrologic modeling: Toward an integrated data assimilation framework, *Water resources research*, 43, 2007.
- Liu, Y., Liu, R., and Chen, J. M.: Retrospective retrieval of long - term consistent global leaf area index (1981 - 2011) from combined AVHRR and MODIS data, *Journal of Geophysical Research: Biogeosciences*, 117, 2012.
- 930 Liu, Y., Xiao, J., Ju, W., Zhou, Y., Wang, S., and Wu, X.: Water use efficiency of China's terrestrial ecosystems and responses to drought, *Scientific reports*, 5, 13799, 2015.
- Liu, Y., Xiao, J., Ju, W., Zhu, G., Wu, X., Fan, W., Li, D., and Zhou, Y.: Satellite-derived LAI products exhibit large discrepancies and can lead to substantial uncertainty in simulated carbon and water fluxes, *Remote Sensing of Environment*, 206, 174-188, 2018.
- 935 Liu, Z., Zhou, Y., Ju, W., and Gao, P.: Simulation of soil water content in farm lands with the BEPS ecological model, *Transactions of the Chinese Society of Agricultural Engineering*, 27, 67-72, 2011.
- Lloyd, J. and Taylor, J.: On the temperature dependence of soil respiration, *Functional ecology*, 315-323, 1994.
- Lorimer, G. and Pierce, J.: Carbonyl sulfide: an alternate substrate for but not an activator of ribulose-1, 5-bisphosphate carboxylase, *Journal of Biological Chemistry*, 264, 2764-2772, 1989.
- 940 Luo, Y., Ogle, K., Tucker, C., Fei, S., Gao, C., LaDeau, S., Clark, J. S., and Schimel, D. S.: Ecological forecasting and data assimilation in a data - rich era, *Ecological Applications*, 21, 1429-1442, 2011.
- Ma, J., Kooijmans, L. M., Cho, A., Montzka, S. A., Glatthor, N., Worden, J. R., Kuai, L., Atlas, E. L., and Krol, M. C.: Inverse modelling of carbonyl sulfide: implementation, evaluation and implications for the global budget, *Atmospheric Chemistry and Physics*, 21, 3507-3529, 2021.
- 945 Ma, R., Xiao, J., Liang, S., Ma, H., He, T., Guo, D., Liu, X., and Lu, H.: Pixel-level parameter optimization of a terrestrial biosphere model for improving estimation of carbon fluxes with an efficient model–data fusion method and satellite-derived LAI and GPP data, *Geoscientific Model Development*, 15, 6637-6657, 2022.
- MacBean, N., Bacour, C., Raoult, N., Bastrikov, V., Koffi, E., Kuppel, S., Maignan, F., Ottlé, C., Peaucelle, M., and Santaren, D.: Quantifying and reducing uncertainty in global carbon cycle predictions: lessons and perspectives from 15 years of data assimilation studies with the ORCHIDEE Terrestrial Biosphere Model, *Global Biogeochemical Cycles*, 36, e2021GB007177, 2022.
- 950 Maignan, F., Abadie, C., Remaud, M., Kooijmans, L. M., Kohonen, K.-M., Commane, R., Wehr, R., Campbell, J. E., Belviso, S., and Montzka, S. A.: Carbonyl sulfide: comparing a mechanistic representation of the vegetation uptake in a land surface model and the leaf relative uptake approach, *Biogeosciences*, 18, 2917-2955, 2021.
- 955 Manzoni, S., Vico, G., Katul, G., Palmroth, S., Jackson, R. B., and Porporato, A.: Hydraulic limits on maximum plant transpiration and the emergence of the safety–efficiency trade - off, *New Phytologist*, 198, 169-178, 2013.
- Medlyn, B. E., Badeck, F. W., De Pury, D., Barton, C., Broadmeadow, M., Ceulemans, R., De Angelis, P., Forstreuter, M., Jach, M., and Kellomäki, S.: Effects of elevated [CO<sub>2</sub>] on photosynthesis in European forest species: a meta - analysis of model parameters, *Plant, Cell & Environment*, 22, 1475-1495, 1999.
- 960 Meredith, L. K., Ogée, J., Boye, K., Singer, E., Wingate, L., von Sperber, C., Sengupta, A., Whelan, M., Pang, E., and Keiluweit, M.: Soil exchange rates of COS and CO<sub>18</sub>O differ with the diversity of microbial communities and their carbonic anhydrase enzymes, *The ISME journal*, 13, 290-300, 2019.

- Monteith, J. and Unsworth, M.: Principles of environmental physics: plants, animals, and the atmosphere, Academic Press 2013.
- 965 Montzka, S., Calvert, P., Hall, B., Elkins, J., Conway, T., Tans, P., and Sweeney, C.: On the global distribution, seasonality, and budget of atmospheric carbonyl sulfide (COS) and some similarities to CO<sub>2</sub>, *Journal of Geophysical Research: Atmospheres*, 112, 2007.
- Moore, J. W. and Schindler, D. E.: Getting ahead of climate change for ecological adaptation and resilience, *Science*, 376, 1421-1426, 2022.
- 970 Niu, S., Luo, Y., Dietze, M. C., Keenan, T. F., Shi, Z., Li, J., and III, F. S. C.: The role of data assimilation in predictive ecology, *Ecosphere*, 5, 1-16, 2014.
- Norton, A. J., Rayner, P. J., Koffi, E. N., and Scholze, M.: Assimilating solar-induced chlorophyll fluorescence into the terrestrial biosphere model BETHY-SCOPE v1. 0: model description and information content, *Geoscientific Model Development*, 11, 1517-1536, 2018.
- 975 Ogée, J., Sauze, J., Kesselmeier, J., Genty, B., Van Diest, H., Launois, T., and Wingate, L.: A new mechanistic framework to predict OCS fluxes from soils, *Biogeosciences*, 13, 2221-2240, 2016.
- Pastorello, G., Trotta, C., Canfora, E., Chu, H., Christianson, D., Cheah, Y.-W., Poindexter, C., Chen, J., Elbashandy, A., and Humphrey, M.: The FLUXNET2015 dataset and the ONEFlux processing pipeline for eddy covariance data, *Scientific data*, 7, 1-27, 2020.
- 980 Peylin, P., Bacour, C., MacBean, N., Leonard, S., Rayner, P., Kuppel, S., Koffi, E., Kane, A., Maignan, F., and Chevallier, F.: A new stepwise carbon cycle data assimilation system using multiple data streams to constrain the simulated land surface carbon cycle, *Geoscientific Model Development*, 9, 3321-3346, 2016.
- Protoschill-Krebs, G., Wilhelm, C., and Kesselmeier, J.: Consumption of carbonyl sulphide (COS) by higher plant carbonic anhydrase (CA), *Atmospheric Environment*, 30, 3151-3156, 1996.
- 985 Prytz, G., Futsaether, C. M., and Johnsson, A.: Thermography studies of the spatial and temporal variability in stomatal conductance of *Avena* leaves during stable and oscillatory transpiration, *New Phytologist*, 158, 249-258, 2003.
- Quirita, V. A. A., da Costa, G. A. O. P., Happ, P. N., Feitosa, R. Q., da Silva Ferreira, R., Oliveira, D. A. B., and Plaza, A.: A new cloud computing architecture for the classification of remote sensing data, *IEEE Journal of Selected Topics in Applied Earth Observations and Remote Sensing*, 10, 409-416, 2016.
- 990 Rastogi, B., Berkelhammer, M., Wharton, S., Whelan, M. E., Iitter, M. S., Leen, J. B., Gupta, M. X., Noone, D., and Still, C. J.: Large uptake of atmospheric OCS observed at a moist old growth forest: Controls and implications for carbon cycle applications, *Journal of Geophysical Research: Biogeosciences*, 123, 3424-3438, 2018.
- Rayner, P. J., Scholze, M., Knorr, W., Kaminski, T., Giering, R., and Widmann, H.: Two decades of terrestrial carbon fluxes from a carbon cycle data assimilation system (CCDAS), *Global biogeochemical cycles*, 19, 2005.
- 995 Reichstein, M., Falge, E., Baldocchi, D., Papale, D., Aubinet, M., Berbigier, P., Bernhofer, C., Buchmann, N., Gilmanov, T., and Granier, A.: On the separation of net ecosystem exchange into assimilation and ecosystem respiration: review and improved algorithm, *Global change biology*, 11, 1424-1439, 2005.
- Remaud, M., Chevallier, F., Maignan, F., Belviso, S., Berchet, A., Parouffe, A., Abadie, C., Bacour, C., Lennartz, S., and Peylin, P.: Plant gross primary production, plant respiration and carbonyl sulfide emissions over the globe inferred by atmospheric inverse modelling, *Atmospheric Chemistry and Physics*, 22, 2525-2552, 2022.
- 1000 Resco de Dios, V., Chowdhury, F. I., Granda, E., Yao, Y., and Tissue, D. T.: Assessing the potential functions of nocturnal stomatal conductance in C<sub>3</sub> and C<sub>4</sub> plants, *New Phytologist*, 223, 1696-1706, 2019.
- Richardson, A. D., Anderson, R. S., Arain, M. A., Barr, A. G., Bohrer, G., Chen, G., Chen, J. M., Ciais, P., Davis, K. J., and Desai, A. R.: Terrestrial biosphere models need better representation of vegetation phenology: results from the North American Carbon Program Site Synthesis, *Global Change Biology*, 18, 566-584, 2012.
- 1005 Rodell, M., Houser, P., Jambor, U., Gottschalck, J., Mitchell, K., Meng, C.-J., Arsenault, K., Cosgrove, B., Radakovich, J., and Bosilovich, M.: The global land data assimilation system, *Bulletin of the American Meteorological society*, 85, 381-394, 2004.
- Rogers, A.: The use and misuse of V<sub>c</sub>, max in Earth System Models, *Photosynthesis research*, 119, 15-29, 2014.
- 1010 Rogers, A., Medlyn, B. E., Dukes, J. S., Bonan, G., Von Caemmerer, S., Dietze, M. C., Kattge, J., Leakey, A. D., Mercado, L. M., and Niinemets, Ü.: A roadmap for improving the representation of photosynthesis in Earth system models, *New Phytologist*, 213, 22-42, 2017.
- Ryu, Y., Jiang, C., Kobayashi, H., and Detto, M.: MODIS-derived global land products of shortwave radiation and diffuse and total photosynthetically active radiation at 5 km resolution from 2000, *Remote Sensing of Environment*, 204, 812-825, 2018.
- 1015 Salmon, E., Jégou, F., Guenet, B., Jourdain, L., Qiu, C., Bastrikov, V., Guimbaud, C., Zhu, D., Ciais, P., and Peylin, P.: Assessing methane emissions for northern peatlands in ORCHIDEE-PEAT revision 7020, *Geoscientific Model Development*, 15, 2813-2838, 2022.
- Sandoval-Soto, L., Stanimirov, M., Von Hobe, M., Schmitt, V., Valdes, J., Wild, A., and Kesselmeier, J.: Global uptake of carbonyl sulfide (COS) by terrestrial vegetation: Estimates corrected by deposition velocities normalized to the uptake of carbon dioxide (CO<sub>2</sub>), *Biogeosciences*, 2, 125-132, 2005.
- 1020 Santaren, D., Peylin, P., Viovy, N., and Ciais, P.: Optimizing a process - based ecosystem model with eddy - covariance flux measurements: A pine forest in southern France, *Global Biogeochemical Cycles*, 21, 2007.

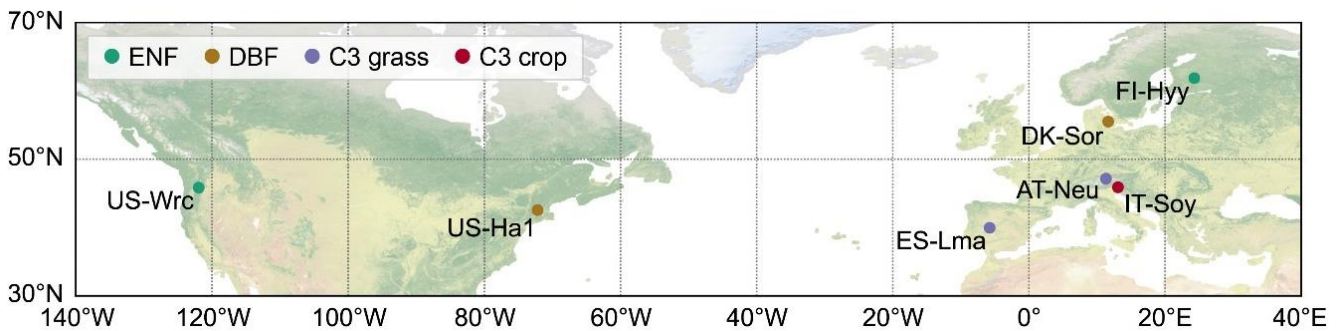


- 1025 Sargsyan, K., Safta, C., Najm, H. N., Debusschere, B. J., Ricciuto, D., and Thornton, P.: Dimensionality reduction for complex models via Bayesian compressive sensing, *International Journal for Uncertainty Quantification*, 4, 2014.
- Sauze, J., Ogée, J., Maron, P.-A., Crouzet, O., Nowak, V., Wohl, S., Kaisermann, A., Jones, S. P., and Wingate, L.: The interaction of soil phototrophs and fungi with pH and their impact on soil CO<sub>2</sub>, CO<sub>18</sub>O and OCS exchange, *Soil Biology and Biochemistry*, 115, 371-382, 2017.
- 1030 Schimel, D., Pavlick, R., Fisher, J. B., Asner, G. P., Saatchi, S., Townsend, P., Miller, C., Frankenberg, C., Hibbard, K., and Cox, P.: Observing terrestrial ecosystems and the carbon cycle from space, *Global Change Biology*, 21, 1762-1776, 2015.
- Scholes, R. J. and Walker, B. H.: *An African savanna: synthesis of the Nylsvley study*, Cambridge University Press 1993.
- Scholze, M., Buchwitz, M., Dorigo, W., Guanter, L., and Quegan, S.: Reviews and syntheses: Systematic Earth observations for use in terrestrial carbon cycle data assimilation systems, *Biogeosciences*, 14, 3401-3429, 2017.
- 1035 Scholze, M., Kaminski, T., Knorr, W., Blessing, S., Vossbeck, M., Grant, J., and Scipal, K.: Simultaneous assimilation of SMOS soil moisture and atmospheric CO<sub>2</sub> in-situ observations to constrain the global terrestrial carbon cycle, *Remote sensing of environment*, 180, 334-345, 2016.
- Scholze, M., Kaminski, T., Knorr, W., Voßbeck, M., Wu, M., Ferrazzoli, P., Kerr, Y., Mialon, A., Richaume, P., and Rodríguez-Fernández, N.: Mean European carbon sink over 2010–2015 estimated by simultaneous assimilation of atmospheric CO<sub>2</sub>, soil moisture, and vegetation optical depth, *Geophysical Research Letters*, 46, 13796-13803, 2019.
- 1040 Schürmann, G. J., Kaminski, T., Köstler, C., Carvalhais, N., Voßbeck, M., Kattge, J., Giering, R., Rödenbeck, C., Heimann, M., and Zaehle, S.: Constraining a land-surface model with multiple observations by application of the MPI-Carbon Cycle Data Assimilation System V1. 0, *Geoscientific Model Development*, 9, 2999-3026, 2016.
- Schwalm, C. R., Williams, C. A., Schaefer, K., Anderson, R., Arain, M. A., Baker, I., Barr, A., Black, T. A., Chen, G., and Chen, J. M.: A model - data intercomparison of CO<sub>2</sub> exchange across North America: Results from the North American
- 1045 Carbon Program site synthesis, *Journal of Geophysical Research: Biogeosciences*, 115, 2010.
- Seibt, U., Kesselmeier, J., Sandoval-Soto, L., Kuhn, U., and Berry, J.: A kinetic analysis of leaf uptake of COS and its relation to transpiration, photosynthesis and carbon isotope fractionation, *Biogeosciences*, 7, 333-341, 2010.
- Shaw, D. C., Franklin, J. F., Bible, K., Klopatek, J., Freeman, E., Greene, S., and Parker, G. G.: Ecological setting of the Wind River old-growth forest, *Ecosystems*, 7, 427-439, 2004.
- 1050 Smith, K. S., Jakubzick, C., Whittam, T. S., and Ferry, J. G.: Carbonic anhydrase is an ancient enzyme widespread in prokaryotes, *Proceedings of the National Academy of Sciences*, 96, 15184-15189, 1999.
- Spielmann, F., Wohlfahrt, G., Hammerle, A., Kitz, F., Migliavacca, M., Alberti, G., Ibrom, A., El - Madany, T. S., Gerdel, K., and Moreno, G.: Gross primary productivity of four European ecosystems constrained by joint CO<sub>2</sub> and COS flux measurements, *Geophysical research letters*, 46, 5284-5293, 2019.
- 1055 Spielmann, F. M., Hammerle, A., Kitz, F., Gerdel, K., and Wohlfahrt, G.: Seasonal dynamics of the COS and CO<sub>2</sub> exchange of a managed temperate grassland, *Biogeosciences*, 17, 4281-4295, 2020.
- Staudt, K., Falge, E., Pyles, R. D., Paw U, K. T., and Foken, T.: Sensitivity and predictive uncertainty of the ACASA model at a spruce forest site, *Biogeosciences*, 7, 3685-3705, 2010.
- 1060 Stimler, K., Berry, J. A., and Yakir, D.: Effects of carbonyl sulfide and carbonic anhydrase on stomatal conductance, *Plant Physiology*, 158, 524-530, 2012.
- Stimler, K., Berry, J. A., Montzka, S. A., and Yakir, D.: Association between carbonyl sulfide uptake and <sup>18</sup>D during gas exchange in C<sub>3</sub> and C<sub>4</sub> leaves, *Plant physiology*, 157, 509-517, 2011.
- Stimler, K., Montzka, S. A., Berry, J. A., Rudich, Y., and Yakir, D.: Relationships between carbonyl sulfide (COS) and CO<sub>2</sub> during leaf gas exchange, *New Phytologist*, 186, 869-878, 2010.
- 1065 Sun, W., Berry, J. A., Yakir, D., and Seibt, U.: Leaf relative uptake of carbonyl sulfide to CO<sub>2</sub> seen through the lens of stomatal conductance–photosynthesis coupling, *New Phytologist*, 235, 1729-1742, 2022.
- Sun, W., Maseyk, K., Lett, C., and Seibt, U.: A soil diffusion–reaction model for surface COS flux: COSSM v1, *Geoscientific Model Development*, 8, 3055-3070, 2015.
- 1070 Sun, W., Kooijmans, L. M., Maseyk, K., Chen, H., Mammarella, I., Vesala, T., Levula, J., Keskinen, H., and Seibt, U.: Soil fluxes of carbonyl sulfide (COS), carbon monoxide, and carbon dioxide in a boreal forest in southern Finland, *Atmospheric Chemistry and Physics*, 18, 1363-1378, 2018.
- Sun, Z., Wang, X., Zhang, X., Tani, H., Guo, E., Yin, S., and Zhang, T.: Evaluating and comparing remote sensing terrestrial GPP models for their response to climate variability and CO<sub>2</sub> trends, *Science of the total environment*, 668, 696-713, 2019.
- 1075 Talagrand, O.: Assimilation of observations, an introduction (gtspecial issue\data assimilation in meteorology and oceanography: Theory and practice), *Journal of the Meteorological Society of Japan. Ser. II*, 75, 191-209, 1997.
- Talagrand, O. and Courtier, P.: Variational assimilation of meteorological observations with the adjoint vorticity equation. I: Theory, *Quarterly Journal of the Royal Meteorological Society*, 113, 1311-1328, 1987.
- Tarantola, A.: *Inverse problem theory : methods for data fitting and model parameter estimation*, 1987.
- Tarantola, A.: *Inverse problem theory and methods for model parameter estimation*, SIAM 2005.
- 1080 Urbanski, S., Barford, C., Wofsy, S., Kucharik, C., Pyle, E., Budney, J., McKain, K., Fitzjarrald, D., Czikowsky, M., and Munger, J.: Factors controlling CO<sub>2</sub> exchange on timescales from hourly to decadal at Harvard Forest, *Journal of Geophysical Research: Biogeosciences*, 112, 2007.
- Verbeeck, H., Samson, R., Verdonck, F., and Lemeur, R.: Parameter sensitivity and uncertainty of the forest carbon flux model FORUG: a Monte Carlo analysis, *Tree physiology*, 26, 807-817, 2006.

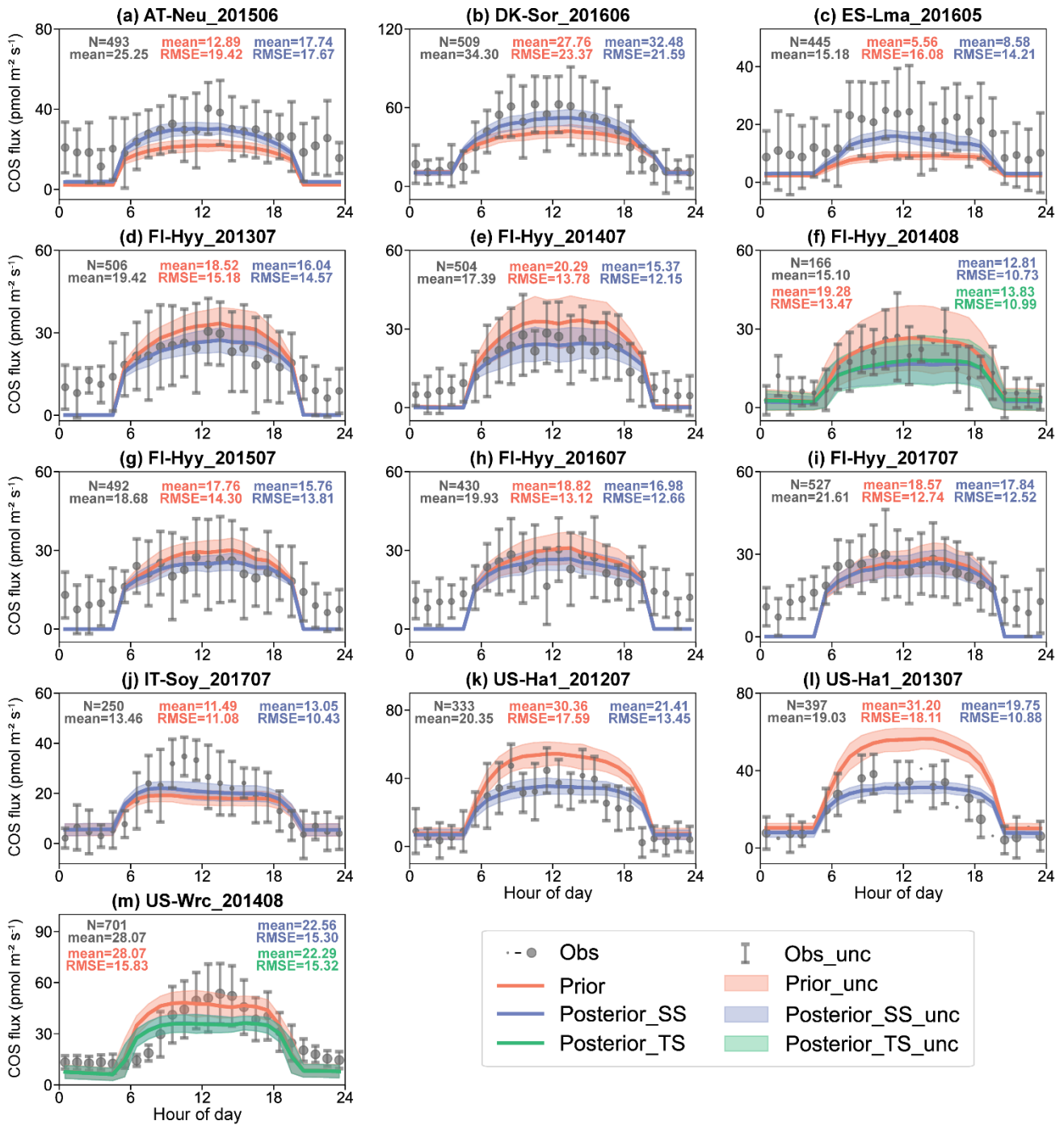
- 1085 Vesala, T., Kohonen, K.-M., Kooijmans, L. M., Praplan, A. P., Foltýnová, L., Kolari, P., Kulmala, M., Bäck, J., Nelson, D., and Yakir, D.: Long-term fluxes of carbonyl sulfide and their seasonality and interannual variability in a boreal forest, *Atmospheric Chemistry and Physics*, 22, 2569-2584, 2022.
- Wang, J., Jiang, F., Wang, H., Qiu, B., Wu, M., He, W., Ju, W., Zhang, Y., Chen, J. M., and Zhou, Y.: Constraining global terrestrial gross primary productivity in a global carbon assimilation system with OCO-2 chlorophyll fluorescence data, *Agricultural and Forest Meteorology*, 304, 108424, 2021.
- 1090 Wang, K.-Y., Kellomäki, S., Zha, T., and Peltola, H.: Component carbon fluxes and their contribution to ecosystem carbon exchange in a pine forest: an assessment based on eddy covariance measurements and an integrated model, *Tree Physiology*, 24, 19-34, 2004.
- Wehr, R., Commane, R., Munger, J. W., McManus, J. B., Nelson, D. D., Zahniser, M. S., Saleska, S. R., and Wofsy, S. C.: Dynamics of canopy stomatal conductance, transpiration, and evaporation in a temperate deciduous forest, validated by carbonyl sulfide uptake, *Biogeosciences*, 14, 389-401, 2017.
- Whelan, M. E. and Rhew, R. C.: Carbonyl sulfide produced by abiotic thermal and photodegradation of soil organic matter from wheat field substrate, *Journal of Geophysical Research: Biogeosciences*, 120, 54-62, 2015.
- Whelan, M. E., Hilton, T. W., Berry, J. A., Berkelhammer, M., Desai, A. R., and Campbell, J. E.: Carbonyl sulfide exchange in soils for better estimates of ecosystem carbon uptake, *Atmospheric Chemistry and Physics*, 16, 3711-3726, 2016.
- 1100 Whelan, M. E., Shi, M., Sun, W., Vries, L. K. d., Seibt, U., and Maseyk, K.: Soil carbonyl sulfide (OCS) fluxes in terrestrial ecosystems: an empirical model, *Journal of Geophysical Research: Biogeosciences*, 127, e2022JG006858, 2022.
- Whelan, M. E., Lennartz, S. T., Gimeno, T. E., Wehr, R., Wohlfahrt, G., Wang, Y., Kooijmans, L. M., Hilton, T. W., Belviso, S., and Peylin, P.: Reviews and syntheses: Carbonyl sulfide as a multi-scale tracer for carbon and water cycles, *Biogeosciences*, 15, 3625-3657, 2018.
- 1105 Wohlfahrt, G., Brilli, F., Hörtnagl, L., Xu, X., Bingemer, H., Hansel, A., and Loreto, F.: Carbonyl sulfide (COS) as a tracer for canopy photosynthesis, transpiration and stomatal conductance: potential and limitations, *Plant, cell & environment*, 35, 657-667, 2012.
- Woodward, F. I., Smith, T. M., and Emanuel, W. R.: A global land primary productivity and phytogeography model, *Global biogeochemical cycles*, 9, 471-490, 1995.
- 1110 Wu, M., Scholze, M., Kaminski, T., Voßbeck, M., and Tagesson, T.: Using SMOS soil moisture data combining CO<sub>2</sub> flask samples to constrain carbon fluxes during 2010–2015 within a Carbon Cycle Data Assimilation System (CCDAS), *Remote Sensing of Environment*, 240, 111719, 2020.
- Wu, M., Scholze, M., Voßbeck, M., Kaminski, T., and Hoffmann, G.: Simultaneous assimilation of remotely sensed soil moisture and FAPAR for improving terrestrial carbon fluxes at multiple sites using CCDAS, *Remote Sensing*, 11, 27, 2018.
- 1115 Wu, Z., Zhang, L., Wang, X., and Munger, J.: A modified micrometeorological gradient method for estimating O<sub>3</sub> dry depositions over a forest canopy, *Atmospheric Chemistry and Physics*, 15, 7487-7496, 2015.
- Xiao, Z., Liang, S., Wang, J., Xiang, Y., Zhao, X., and Song, J.: Long-time-series global land surface satellite leaf area index product derived from MODIS and AVHRR surface reflectance, *IEEE Transactions on Geoscience and Remote Sensing*, 54, 5301-5318, 2016.
- 1120 Yu, K., Goldsmith, G. R., Wang, Y., and Anderegg, W. R.: Phylogenetic and biogeographic controls of plant nighttime stomatal conductance, *New Phytologist*, 222, 1778-1788, 2019.
- Zaehle, S., Sitch, S., Smith, B., and Hatterman, F.: Effects of parameter uncertainties on the modeling of terrestrial biosphere dynamics, *Global Biogeochemical Cycles*, 19, 2005.
- 1125 Zhu, H., Xing, X., Wu, M., Ju, W., and Jiang, F.: Optimizing the terrestrial ecosystem gross primary productivity using carbonyl sulfide (COS) within a “two-leaf” modeling framework, *EGU sphere*, 2024, 1-34, 2024.
- Zierl, B.: A water balance model to simulate drought in forested ecosystems and its application to the entire forested area in Switzerland, *Journal of Hydrology*, 242, 115-136, 2001.
- 1130 Zobitz, J., Moore, D. J., Quaipe, T., Braswell, B. H., Bergeson, A., Anthony, J. A., and Monson, R. K.: Joint data assimilation of satellite reflectance and net ecosystem exchange data constrains ecosystem carbon fluxes at a high-elevation subalpine forest, *Agricultural and Forest Meteorology*, 195, 73-88, 2014.



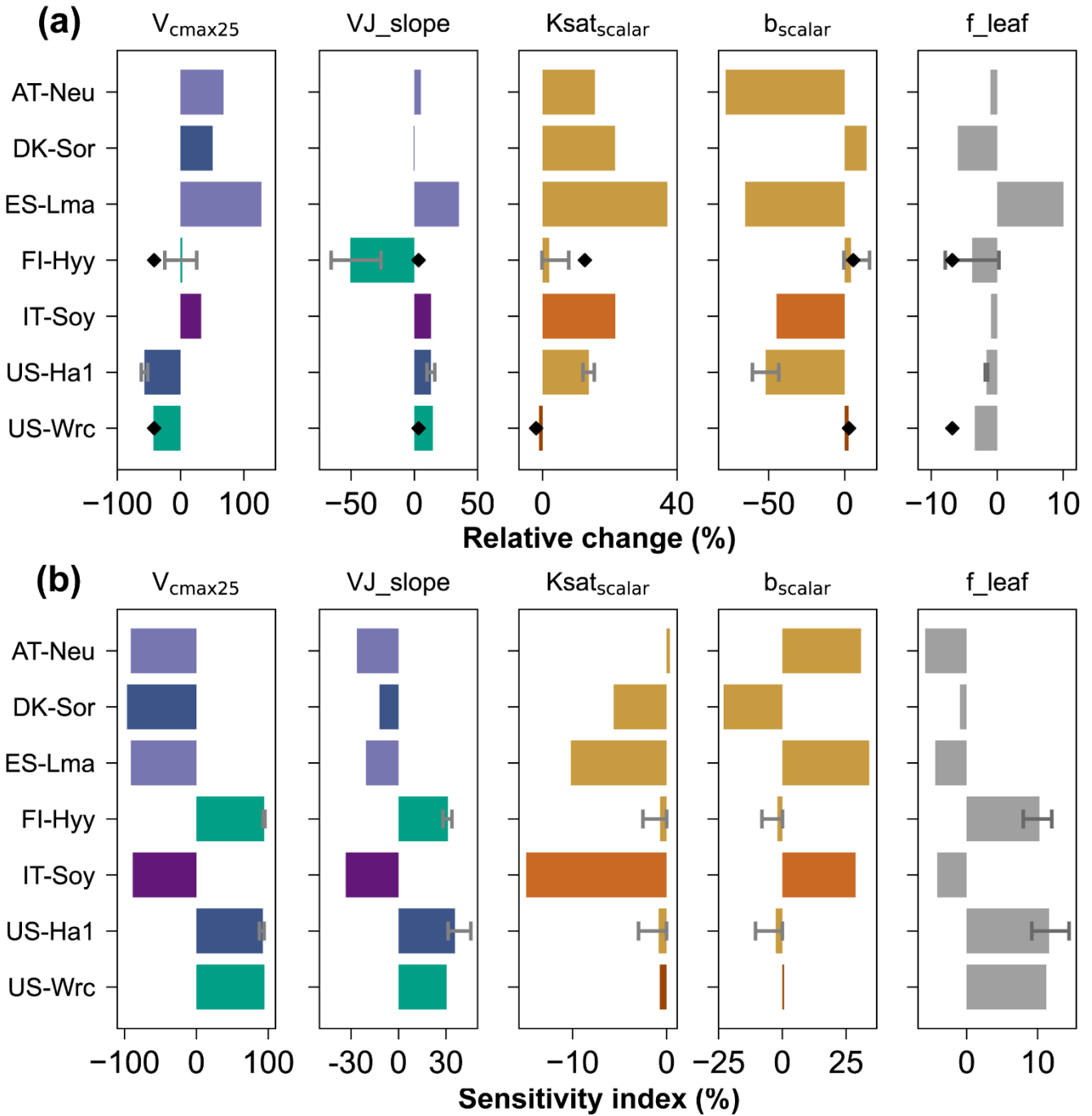
1135 **Figure 1.** Schematic of the Nanjing University Carbon Assimilation System (NUCAS). Left: illustration of a two-leaf model coupling stomatal conductance, photosynthesis, transpiration and COS uptake, and an empirical model for simulating soil COS fluxes in NUCAS. Right: data assimilation flowchart of NUCAS. Ovals represent input (blue-grey) and output data (green). Boxes and the rhombi represent the calculation and judgement steps. The solid black line represents the diagnostic process, the solid blue line represents the prognostic process, and the input datasets of BEPS (in the dashed box) are used in both diagnostic process and prognostic process.



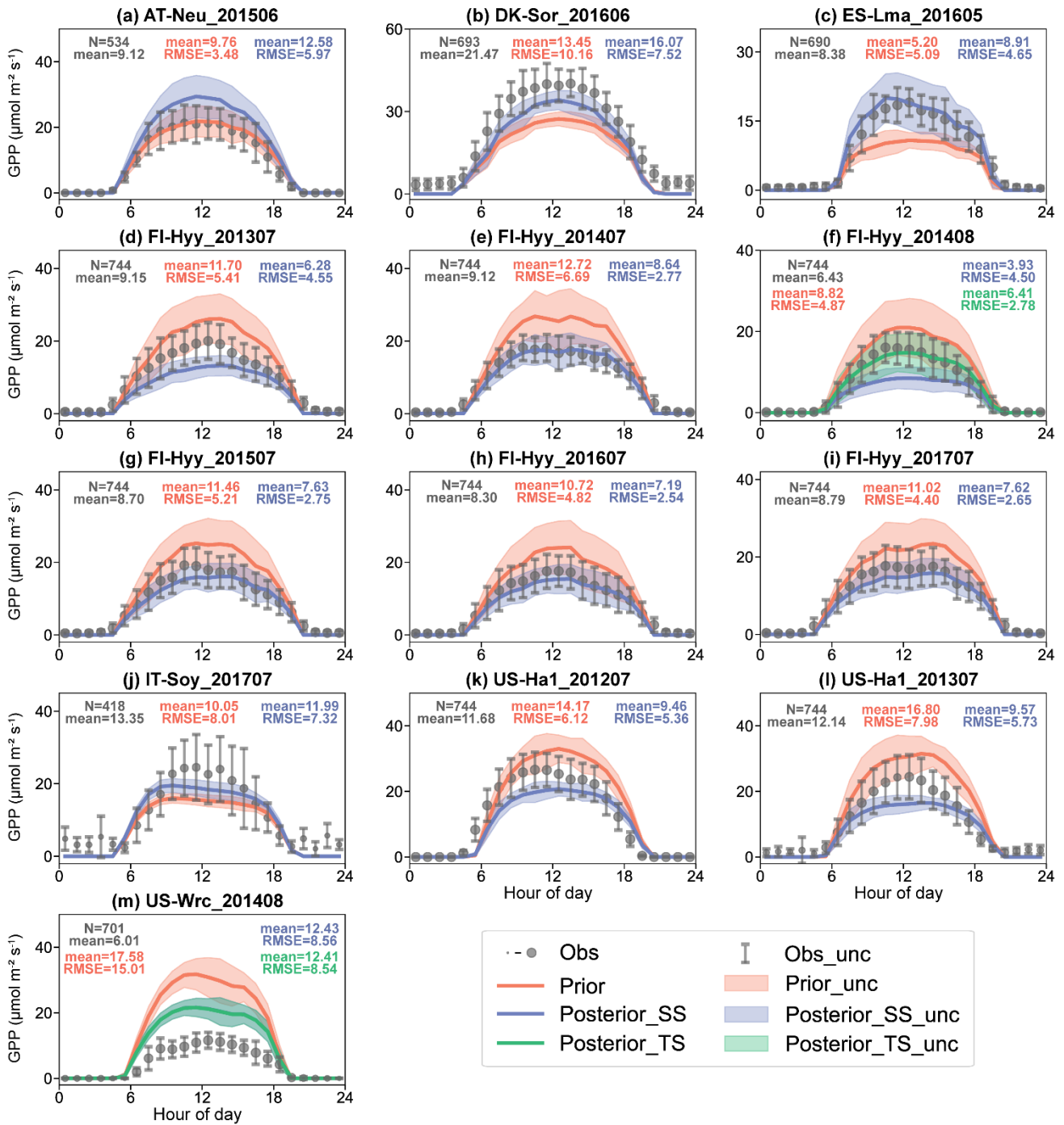
1140 **Figure 2.** Locations of the 7 studied sites. Sites sharing the same plant function type are represented with consistent colors. The background map corresponds to the "Nature color I" map (<https://www.natureearthdata.com>). ENF and DBF denote evergreen needleleaf forest and deciduous broadleaf forest, respectively.



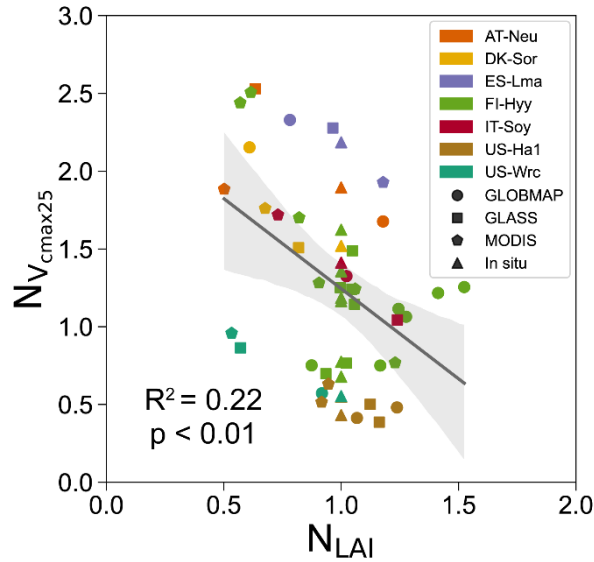
1145 **Figure 3.** The mean diurnal cycle of observed (blue) and simulated COS flux using prior parameters (red) and single-site posterior parameters (blue). The size of the circle indicates the number of observations (ranging from 1 to 31) within each circle, and the error bars depict the standard deviations in the mean of observations from the variability within each circle if the number of corresponding observations is greater than three. Lines connect the mean values of simulations and pale bands depict the standard deviation in the mean of simulations from the variability within each bin.



1150 **Figure 4.** (a) Relative changes of parameters for single-site experiments (bars) and the multi-site experiment (diamond points). (b) Sensitivity indexes of parameters at prior values. For sites where multiple single-site experiments were conducted, the ends of the error bars and the bar indicate the maximum, minimum and mean of the relative changes of the parameters, respectively. For those sites lacking multi-year COS observations, no error bars were plotted. The color of bar is drawn according to PFT/texture.



1155 **Figure 6.** The diurnal cycle of observed (blue) and simulated GPP using prior parameters (red), single-site (green) and multi-site (brown) posterior parameters. The size of the circle indicates the number of observations within each circle (ranging from 1 to 31), and the error bars depict the standard deviations in the mean of observations from the variability within each circle. Lines connect the mean values of simulations and pale bands depict the standard deviation in the mean of simulations from the variability within each bin.



1160 **Figure 7.** Influence of LAI on the posterior  $V_{cmax25}$  obtained by the single-site experiments conducted at seven sites and driven by four LAI  
 1165 data (GLOBMAP, GLASS, MODIS and *in situ*). The posterior  $V_{cmax25}$  and the LAI were represented by their normalized values  $N_{V_{cmax25}}$   
 and  $N_{LAI}$ , respectively. The posterior parameters were normalized by their prior values and the LAI were normalized by the *in situ* values.  
 The linear regression fit line of the posterior parameters obtained based on the satellite-derived LAI (GLOBMAP, GLASS and MODIS)  
 with the corresponding LAI data is shown, with 95% confidence interval spread around the line.

**Table 1.** Site characteristics. Site identification includes the country initials and a three-letter name for each site; locations of the sites are  
 provided by the latitude (Lat) and longitude (Lon); PFTs covered by the sites are evergreen needleleaf forest (ENF), deciduous broadleaf  
 forest (DBF), C3 grass and C3 crop; Soil texture covered by the sites are sandy loam, slit loam and loam.

Site name	AT-Neu	DK-Sor	ES-Lma	FI-Hyy	IT-Soy	US-Ha1	US-Wrc
Lat (°N)	47.12	55.49	39.94	61.85	45.87	42.54	45.82
Lon (°E)	11.32	11.64	-5.77	24.29	13.08	-72.17	-121.95
PFT	C3 grass	DBF	C3 grass	ENF	C3 crop	DBF	ENF
Soil texture	Sandy loam	Sandy loam	Sandy loam	Sandy loam	Slit loam	Sandy loam	Loam
LAI*	3.88	5.0	1.82	4.0	2.3	5.0	8.7
Year	2015	2016	2016	2013-2017	2017	2012-2013	2014
References	(Spielmann et al., 2020)	(Spielmann et al., 2019)	(Spielmann et al., 2019)	(Sun et al., 2018; Vesala et al., 2022; Kohonen et al., 2022)	(Spielmann et al., 2019; Abadie et al., 2022)	(Commane et al., 2015; Wehr et al., 2017)	(Shaw et al., 2004; Rastogi et al., 2018)

\* Mean one-sided LAI ( $m^2 m^{-2}$ ) during the experimental period

1170 **Table 2.** The configuration and the relative changes (%) of the parameters for each single-site assimilation experiment. The cost function  
 reduction of each experiment is indicated by the reduction rate between the initial value of cost function ( $J_{initial}$ ) and the final value of cost  
 function ( $J_{final}$ ), defined as  $1 - J_{final}/J_{initial}$ , and  $N_{COS}$  denotes the number of ecosystem COS flux observations.

Site name	Assimilation window	$N_{COS}$	Cost function reduction (%)	Relative change (%) of parameters				
				$V_{cmax25}$	VJ_slope	$K_{sat_{scalar}}$	$b_{scalar}$	f_leaf
AT-Neu	June 2015	493	16.39	67.69	5.10	15.57	-78.13	-1.01
DK-Sor	June 2016	509	9.46	50.77	-0.47	21.54	14.23	-5.97
ES-Lma	May 2016	445	15.70	127.80	35.18	37.08	-65.33	10.05
	July 2013	506	5.88	25.50	-65.70	0.37	4.25	-7.89
FI-Hyy	July 2014	504	20.17	-24.96	-26.39	3.82	16.24	-6.12
	August 2014	166	38.86	-24.84	-56.81	7.79	4.46	-1.52
	July 2015	492	5.53	6.43	-50.25	0.01	-0.06	0.26
	July 2016	430	4.37	11.47	-53.16	-0.17	-0.63	-0.37
	July 2017	527	2.84	21.70	-51.74	0.01	0.01	-6.98
IT-Soy	July 2017	250	6.35	-7.88	-21.20	0.03	-0.45	-4.14

US-Ha1	July 2012	333	44.14	-51.89	16.08	12.05	-43.31	-1.44
	July 2013	397	63.73	-58.67	10.16	16.93	-58.33	-1.71
US-Wrc	August 2014	701	27.71	-42.77	14.52	-1.04	2.45	-3.39

**Table 3.** The configuration and the relative changes (%) of the parameters for the multi-site assimilation experiment at FI-Hyy and US-Wrc.  $N_{COS}$  denotes the total number of ecosystem COS flux observations.

Site name	Assimilation window	$N_{COS}$	Cost function reduction (%)	Relative change (%) of parameters				
				$V_{cmax25}$	VJ_slope	$Ksat_{scalar}$	$b_{scalar}$	f_leaf
FI-Hyy	August 2014	867	28.17	-41.74	3.36	12.57	5.57	-6.81
US-Wrc				-1.91	2.75			

1175

### Appendix: Stomatal conductance and soil hydrology modelling in BEPS, including parameters to be optimised

In BEPS model, the leaf stomatal conductance to water vapor ( $g_{sw}$  in  $\text{mol m}^{-2} \text{s}^{-1}$ ) is estimated using a modified version of Ball-Berry empirical model (Ball et al., 1987) following Woodward et al. (1995):

$$g_{sw} = b_{H_2O} + \frac{m_{H_2O} A R_h f_w}{C_a} \quad (\text{A1})$$

1180

where  $b_{H_2O}$  is the intercept of the BB model, representing the minimum  $g_{sw}$  ( $\text{mol m}^{-2} \text{s}^{-1}$ ),  $m_{H_2O}$  is the empirical slope parameter in the BB model (unitless),  $R_h$  is the relative humidity at the leaf surface (unitless),  $f_w$  is a soil moisture stress factor describing the sensitivity of  $g_{sw}$  to soil water availability (Ju et al., 2006),  $C_a$  is the atmospheric  $\text{CO}_2$  concentration ( $\mu\text{mol mol}^{-1}$ ), and the net photosynthesis rate (A) is calculated using the Farquhar model (Farquhar et al., 1980; Chen et al., 1999):

1185

$$A = \min(A_i, A_j) - R_d \quad (\text{A2})$$

$$A_c = V_{cmax} \frac{C_i - \Gamma_i^*}{C_i + K_c \left(1 + \frac{O_i}{K_o}\right)} \quad (\text{A3})$$

$$A_j = J \frac{C_i - \Gamma_i^*}{4(C_i - 2\Gamma_i^*)} \quad (\text{A4})$$

1190

where  $A_i$  and  $A_j$  are Rubisco-limited and RuBP-limited gross photosynthetic rates ( $\mu\text{mol m}^{-2} \text{s}^{-1}$ ), respectively.  $R_d$  is leaf dark respiration ( $\mu\text{mol m}^{-2} \text{s}^{-1}$ ).  $V_{cmax}$  is the maximum carboxylation rate of Rubisco ( $\mu\text{mol m}^{-2} \text{s}^{-1}$ ); J is the electron transport rate ( $\mu\text{mol m}^{-2} \text{s}^{-1}$ );  $C_i$  and  $O_i$  are the intercellular carbon dioxide ( $\text{CO}_2$ ) and oxygen ( $\text{O}_2$ ) concentrations ( $\text{mol mol}^{-1}$ ), respectively;  $K_c$  and  $K_o$  are Michaelis–Menten constants for  $\text{CO}_2$  and  $\text{O}_2$  ( $\text{mol mol}^{-1}$ ), respectively.

The electron transport rate, J, is dependent on incident photosynthetic photon flux density (PPFD,  $\mu\text{mol m}^{-2} \text{s}^{-1}$ ) as:

$$J = \frac{J_{max} I}{I + 2.1J_{max}} \quad (\text{A5})$$

1195

where  $J_{max}$  is the maximum electron transport rate ( $\mu\text{mol m}^{-2} \text{s}^{-1}$ ),  $I$  is the incident PPFD calculated from the incident shortwave radiation  $R_{sw}$  ( $\text{W m}^{-2}$ ):

$$I = \beta R_{sw} f_{leaf} \quad (\text{A6})$$

where  $\beta = 4.55$  is the energy – quanta conversion factor ( $\mu\text{mol J}^{-1}$ ),  $f_{leaf}$  is the ratio of photosynthesis active radiation to the shortwave radiation (unitless).

1200

The maximum carboxylation rate of Rubisco  $V_{cmax}$  was calculated according the Arrhenius temperature function and the maximum carboxylation rate of Rubisco at 25 °C ( $V_{cmax25}$ ).  $V_{cmax}$  is generally proportional to leaf nitrogen content. Considering both the fractions of sunlit and shaded leaf areas to the total leaf area and the leaf nitrogen content vary with the depth into the canopy, the  $V_{cmax}$  values of sunlit ( $V_{cmax,sun}$ ) and shaded ( $V_{cmax,sh}$ ) leaves can be obtained through vertical integrations with respect to leaf area index (Chen et al., 2012):



$$V_{cmax,sunlit} = V_{cmax}\chi_n N_{leaf} \frac{k[1 - e^{(k_n+k)LAI_{sunlit}}]}{(k_n + k)(1 - e^{-kLAI_{sunlit}})} \quad (A7)$$

1205

$$V_{cmax,shaded} = V_{cmax}\chi_n N_{leaf} \frac{\frac{1}{k_n}[1 - e^{-k_n L}] - \frac{1}{k_n + k}[1 - e^{(k_n+k)LAI_{shaded}}]}{LAI_{shaded} - \frac{1}{k}(1 - e^{-kLAI_{shaded}})} \quad (A8)$$

where  $\chi_n$  ( $m^2 g^{-1}$ ) is the relative change of  $V_{cmax}$  to leaf nitrogen content;  $N_{leaf}$  ( $g m^{-2}$ ) is the leaf nitrogen content at the top of the canopy;  $k_n$  (unitless) is the leaf nitrogen content decay rate with increasing depth into the canopy, taken as 0.3;  $k$  is calculated as:

$$k = G(\theta)\Omega \cos(\theta) \quad (A9)$$

1210

where  $G(\theta)$  is the projection coefficient, taken as 0.5,  $\Omega$  is the clumping index, and  $\theta$  is the solar zenith angle.

After  $V_{cmax}$  values for the representative sunlit and shaded leaves are obtained, the maximum electronic transport rate for the sunlit and shaded leaves are obtained from Medlyn et al. (1999):

$$J_{max} = VJ\_slope V_{cmax} - 14.2 \quad (A10)$$

Soil water availability factor  $f_{w,i}$  in each layer  $i$  is calculated as:

1215

$$f_{w,i} = \frac{1.0}{f_i(\psi_i)f_i(T_{s,i})} \quad (A11)$$

where  $f_i(\psi_i)$  is a function of matrix suction  $\psi_i$  (m) (Zierl, 2001),  $f_i(T_{s,i})$  is a function describing the effect of soil temperature ( $T_{s,i}$  in °C) on soil water uptake (Bonan, 1991).

To consider the variable soil water potential at different depths, the scheme of Ju et al. (2006) was employed to calculate the weight of each layer ( $w_i$ ) to  $f_w$ :

1220

$$w_i = \frac{R_i f_{w,i}}{\sum_{i=1}^n R_i f_{w,i}} \quad (A12)$$

where  $n$  is the number of soil layer (five were used in this study) of the BEPS model,  $R_i$  is the root fraction in layer  $i$ , calculated as:

$$R_i = \begin{cases} 1 - r_{decay}^{100cd_i} & i = 1 \\ r_{decay}^{100cd_{i-1}} - r_{decay}^{100cd_i} & 1 < i < n \\ r_{decay}^{100cd_{i-1}} & i = n \end{cases} \quad (A13)$$

where  $cd_i$  is the cumulative depth (m) of layer  $i$ . In this study, each soil layer depth (from top to bottom) of the BEPS model is 0.05 m, 0.10 m, 0.20 m, 0.40 m and 1.25 m, respectively.

The overall soil water availability  $f_w$  is then calculated as:

$$f_w = \sum_{i=1}^n f_{w,i} w_i \quad (A14)$$

The hydraulic conductivity of each soil layer  $K_i$  ( $m s^{-1}$ ) is expressed as:

$$K_i = Ksat_i \left( \frac{SWC_i}{\theta_{s,i}} \right)^{2b_i+3} \quad (A15)$$

1230

where  $Ksat_i$  is the saturated hydrological conductivity of soil layer  $i$  ( $m s^{-1}$ );  $SWC_i$  is the volumetric liquid soil water content of soil layer  $i$  ( $m^3 m^{-3}$ );  $\theta_{s,i}$  is the porosity of soil layer  $i$  (unitless);  $b_i$  is the Campbell parameter for soil layer  $i$ , determining the change rate of hydraulic conductivity with SWC (unitless). In this study,  $Ksat_i$  and  $b_i$  are expressed as:

$$Ksat_i = Ksat_{scalar} Ksat_{df,i} \quad (A16)$$

$$b_i = b_{scalar} b_{df,i} \quad (A17)$$

1235

where  $Ksat_{df,i}$  and  $b_{df,i}$  are the default values of  $Ksat_i$  and  $b_i$  respectively.